Journal of Iberian Geology **41 (2) 2015:** 233-252
http://dx.doi.org/10.5209/rev_JIGE.2015.v41.n2.47617

www.ucm.es/info/estratig/journal.htm
ISSN (print): 1698-6180. ISSN (online): 1886-7995

Journal of Iberian Geology
AN INTERNATIONAL PUBLICATION OF EARTH SCIENCES

Gravity modeling of the lithosphere in the Calatrava Volcanic Province (Spain): geodynamic implications

J.L. Granja Bruña[1,*], R. Vegas[1], M.A. Sentre Domingo[2], A. Muñoz-Martín[1,3], S. Sainz-Maza Aparicio[2]

[1]*Applied Tectonophysics Group. Departamento de Geodinámica. Universidad Complutense de Madrid. 28040, Madrid, Spain.*
[2]*Observatorio Geofísico Central. Instituto Geográfico Nacional. 28014, Madrid, Spain.*
[3]*Instituto de Geociencias IGEO (CSIC, UCM). C./ José Antonio Nováis, 12, 28040 Madrid, Spain*

*e-mail addresses: jlgranja@ucm.es (J.L.G.B.; *corresponding author); ruidera@ucm.es (R.V.M.); sentredomingo@gmail.com (M.A.S.D.); amunoz@ucm.es (A.M.M.); ssainz-maza@fomento.es (S.S.M.A)*

Received: 12 January 2015 / Accepted: 5 July 2015 / Available online: 20 July 2015

Abstract

The origin of the intraplate volcanism in the Calatrava Volcanic Province (CVP) is controversial. On the basis of its geochemical signature, it has been ascribed to an "aborted" rift, implying lithospheric thinning. However, the volcanism occurred during the generalized Cenozoic NW−SE-oriented compressive tectonic regime. On the other hand, on the basis of evidence for its deep-seated origin, it has been linked to the existence of a baby-plume detached from an active megaplume below the Canary-Azores Islands and the western Mediterranean. In order to understand better the aforementioned geodynamic scenarios for the origin of the CVP, we address here the study of the lithosphere in the CVP and its vicinity by means of gravity analysis and 2+1/2D modeling. Gravity modeling results do not support the rifting model adopted for the intraplate volcanism occurred in the CVP because the crust shows a quasi-constant thickness. Density models suggest the existence of a sub-crustal, anomalous low-density block that could be underplated magmatic material at the base of the crust, suggesting that only a minor part of it intruded up into the crust and erupted. The localized magmatism of the CVP can be related to the combination of two factors: active, the gentle folding of the Iberian lithosphere and associated uplifting of the Variscan basement due to the NW-directed transmission of compressive stresses in the upper plate yielded by the subduction/collision in the south Iberian margin. The formation of the lithospheric folding in the Calatrava region results in a decrease of the pressure beneath the swell of the antiform that is likely to bring about basaltic magmatism below the swell; and one passive, the existence of a Variscan right-lateral shear band, which yields a weakened crust that facilitates the ascent of the magmatic materials. The relatively small volume, but large extension, of the volcanic outcrops could be associated with the preferential ascent of the magmas along the weakened crust of this NW−SE-trending Variscan shear band.

Keywords: Calatrava, intraplate volcanism, gravity modeling, lithosphere structure, upward continuation

Resumen

El origen del volcanismo intraplaca en la Provincia Volcánica de Calatrava (CVP) es controvertido. En base a su signatura geoquímica se ha atribuido a la formación de un rift "abortado", implicando un adelgazamiento litosférico. Sin embargo, el volcanismo se desarrolló durante un régimen tectónico compresivo orientado NW-SE que fue generalizado en la región de Calatrava durante el Cenozoico. Por otro lado, en base a las evidencias de su origen profundo, se le ha relacionado con la existencia de una mini-pluma desconectada de una mega-pluma activa debajo de los archipiélagos de Canarias y Azores, y en el Mediterráneo occidental. Con el propósito de contribuir a la discriminación entre los escenarios geodinámicos mencionados para el origen del volcanismo se ha abordado aquí el estudio de la litosfera en la CVP y en las zonas próximas mediante el análisis gravimétrico y la modelación 2+1/2D. Los modelos gravimétricos no apoyan el modelo de rifting adoptado para el volcanismo intraplaca ocurrido en la CVP porque el espesor de la corteza es cuasi-constante. Los modelos siguieren la existencia de un cuerpo anómalo sub-cortical de baja densidad que podría ser material magmático acrecionado y almacenado en la base de la corteza indicando que sólo una parte menor habría intruido en la corteza y producido erupciones. El volcanismo localizado de la CVP se puede relacionar con la combinación de dos factores: a) Un factor activo correspondiente a un amplio plegamiento de la litosfera (corteza) Ibérica y el consiguiente levantamiento asociado del basamento varisco debido a la transmisión hacia el NW de los esfuerzos compresivos en la placa superior de la subducción/colisión miocena en el margen meridional Ibérico. La formación del anticlinal a escala cortical en la región de Calatrava ha producido la disminución de la presión en el intrados del anticlinal y ha originado probablemente el magmatismo basáltico; b) Un factor pasivo correspondiente a la existencia de una banda de cizalla con dirección próxima a NW-SE, heredada de la deformación varisca, que localiza una zona de debilidad cortical favorecedora del ascenso del magmatismo.

Palabras clave: Calatrava, volcanismo intraplaca, modelación gravimétrica, estructura litosférica, prolongación ascendente

1. Introduction

The origin of intraplate volcanism - in particular in retroarc foreland regions and far from subduction zones - is controversial (*e.g.*, Foulger, 2010). This is the case of the Calatrava Volcanic Province in Central Spain (CVP in current literature), which has been included in the so-called Cenozoic Circum-Mediterranean anorogenic igneous province (Fig. 1; Lustrino and Wilson, 2007, and references therein). On the basis of its geochemical signature, the CVP has been ascribed to an "aborted" rift (López-Ruiz *et al.*, 1993), implying crustal thinning and associated, shallow-rooted magmatism during the Late Miocene, when the main phase of volcanism occurred (Ancochea *et al.*, 1979). Nevertheless, a generalized NW−SE-oriented compressive tectonic regime during the Cenozoic, as well as regional physiographic and tectonic analysis, has been argued for a flexural model of the crust and lithosphere being responsible for the foreland setting of the CVP (Vegas and Rincón-Calero, 1996). More recently, on the basis of evidence for its deep-seated origin (Humphreys *et al.*, 2010), it has been linked to the existence of a hot finger (or baby-plume) detached from an active megaplume below the Canary and Azores Islands and the western Mediterranean Sea (Stoppa *et al.*, 2012).

Intraplate volcanism in compressive regimes has been recently suggested to be driven by the compression near collisional/subduction plate boundaries that causes lithospheric folding of the foreland region, resulting in a decrease of the pressure beneath the swell of the antiform while the pressure beneath the synform increases (Shin *et al.*, 2012). The decompression beneath the lithosphere is likely to lead to basaltic magmatism along and below the swell of the antiform. Lithospheric folding of Iberia due to horizontal loading driven by the Alpine orogeny has been suggested from numerical and analogue modeling (*e.g.*, Cloetingh *et al.*, 2002; Muñoz-Martín *et al.*, 2010; Fernández-Lozano *et al.*, 2012). The topography of the center and western part of the Iberian Peninsula shows an alternation of E−W- to NE−SW-trending ridges and troughs that are the surface expression of a succession of crustal folds (*i.e.,* succession of long-wavelength anticlines and synclines) formed perpendicular to the main axis of present-day intraplate NW−SE-trending compression (Muñoz-Martín *et al.*, 2012). La Mancha basin (LMB), where the CVP is located (Fig. 2), is situated in the central zone of a broad swell (*i.e.,* anticline) flanked by the Toledo Mountains and the Sierra Morena located between the NNE−SSW-trending Guadalquivir and Tagus basins (*i.e.,* syncline).

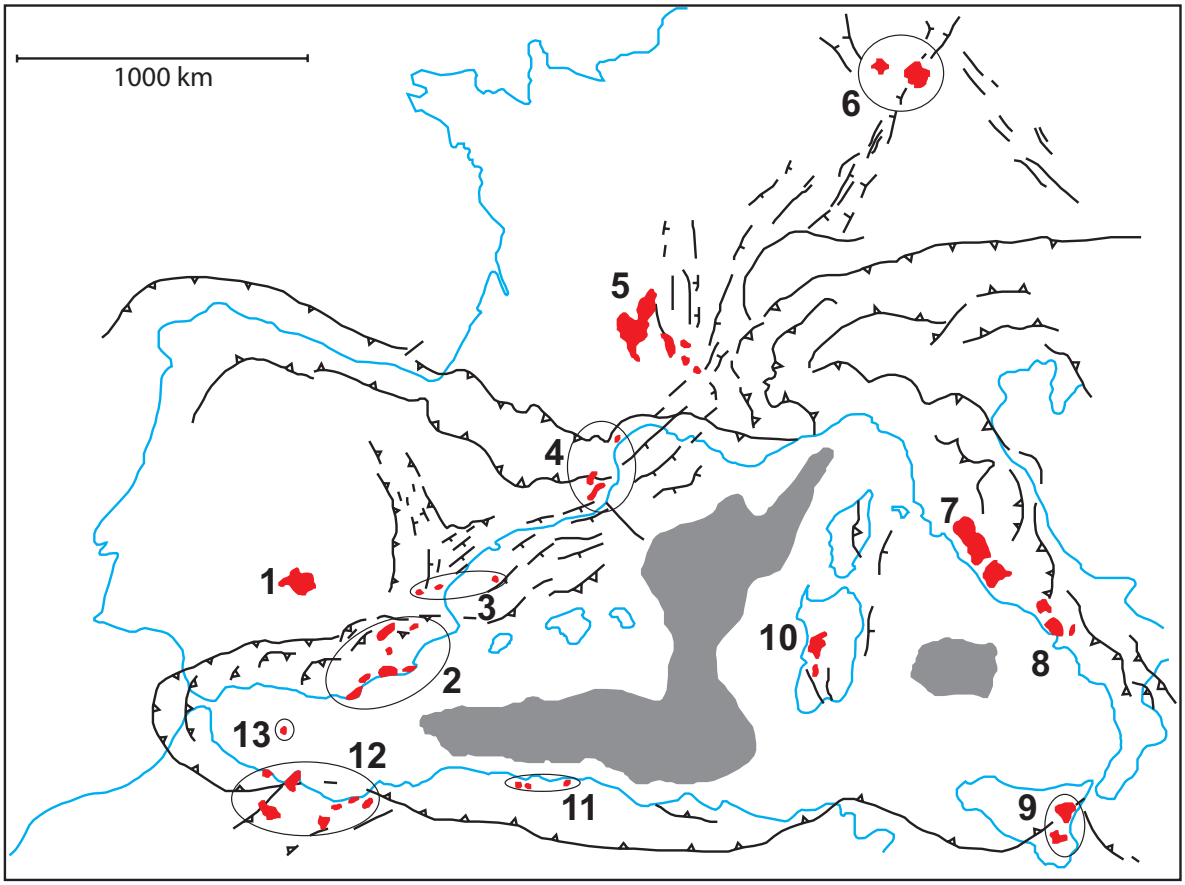

Fig. 1.- **A)** Synthesized map showing the Cenozoic Circum-Mediterranean anorogenic igneous province (Lustrino and Wilson, 2007) and the main structures developed in the Alpine orogeny. Red zones show the Neogene-Quaternary volcanic provinces in and around the western Mediterranean. Light grey zones show oceanic crust. 1= Calatrava. 2= South East Spain. 3= Columbretes Is.-Cofrentes. 4= Olot-Garrotxa, Agde. 5= Massif Central, Limagne. 6= Eifel, Vogelsberg. 7= Tuscany. 8= Rome. 9= Etna, Hyblean Plateau. 10= Sardinia. 11= Tell Mts. 12= Cape Trois Fourches. 13= Alboran Is.

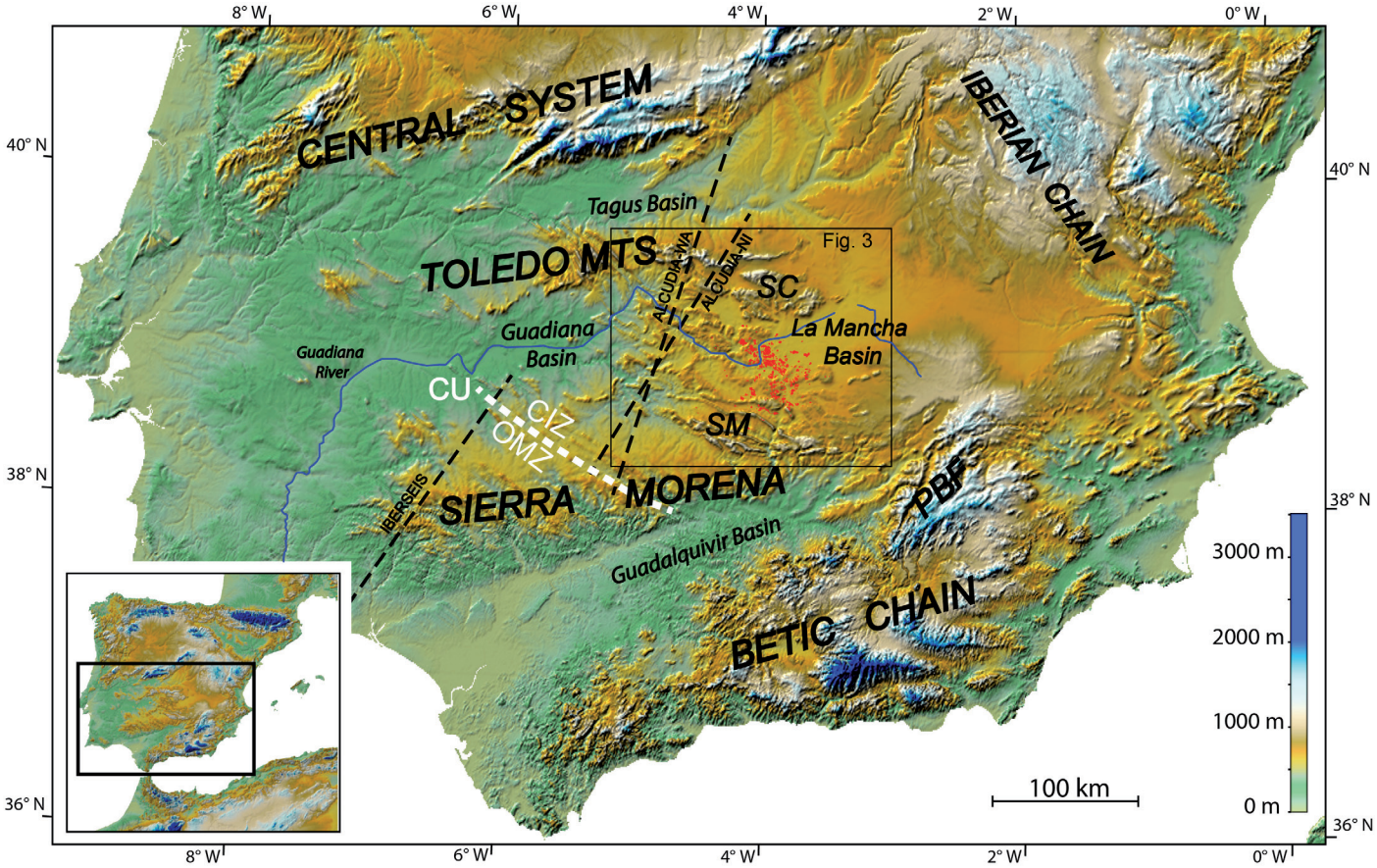

Fig. 2.- Digital elevation model (SRTM90) of the southern Iberian Peninsula showing the swell in the Calatrava region. See inset map for location. Red-colored zones show the volcanic outcrops in the Calatrava Volcanic Province (Ancochea *et al.*, 2004; Cebriá *et al.*, 2011; Sentre Domingo *et al.*, 2014). The dashed black lines show the approximate location of the deep seismic profiles: IBERSEIS (Palomeras *et al.*, 2009), ALCUDIA normal incidence (ALCUDIA-NI; Martínez Poyatos *et al.*, 2012; Simancas *et al.,* 2013; Ehsan *et al.,* 2014) and ALCUDIA wide-angle (ALCUDIA-WA; Ehsan *et al.,* 2015). SC= Sierra de la Calderina. SM= Sierra Madrona. PBF= Prebetic Front. CIZ= Central Iberian Zone. OMZ= Ossa-Morena Zone. The dashed white line shows the approximate location of boundary between the CIZ and the OMZ, known as the Central Unit (CU; Azor *et al.,* 1994). The rectangle shows the location of figure 3.

In order to understand better the aforementioned geodynamic scenarios for the origin of the CVP (*i.e.*, "aborted" rift *vs.* lithospheric folding), we address here the study of the geometry of the Moho and lithosphere-asthenosphere interfaces in the CVP and its vicinity by means of gravity analysis and 2+1/2D modeling. Gravity models have been constrained by deep seismic soundings (Martínez Poyatos *et al.*, 2012; Simancas *et al.,* 2013, Ehsan *et al.,* 2014, 2015) and 3D seismic tomography (Palomeras *et al.*, 2014), as well as by potential field modeling (Bergamín and Carbó, 1986; Sentre Domingo *et al.*, 2014; García-Lobón *et al.*, 2014; Ehsan *et al.,* 2015). Finally, we explore the inclusion of the gravity models into the conceptual model of Shin *et al.* (2012) for the basaltic magmatism occurring in an intraplate, compressive regime.

2. Tectonic setting

The CVP spreads over an area of ≈5000 km^2 in the form of ≈200 individual centers of emission (Ancochea, 1999). This volcanic province occupies a roughly NNE-directed basement uplift framed to the south and north by the Sierra Morena and the Toledo Mountains respectively (Fig. 2). This basement uplift, as a whole, represents a swell between the semi-endorreic La Mancha Basin and the Middle Guadiana Basin. Volcanoes are mostly aligned NW−SE (Ancochea and Brändle, 1982; Cebriá, 1992; Stoppa *et al.*, 2012) and occur over both basement rocks and a thin cover of sediments. The volcanic activity occurred between the Late Miocene and the Early Pleistocene, with two different episodes (Ancochea, 1999): an ultra-potassic episode between 8.7 and 6.4 Ma and an ultra-alkaline episode between 3.7 and 1.75 Ma.

The basement of the Calatrava region forms part of the Central Iberian Zone (CIZ), a tectonic division of the Variscan Iberian Massif, in particular the subdivision characterized by upright and continuous folds (Díez Balda and Vegas, 1992). In the CVP and surrounding areas these folds correspond to paired anticlines and synclines (Vegas and Roiz, 1979), well shown by the Lower Ordovician, erosion-resistant quartzite level, the Armorican Quartzite, which rules the regional physiography of the basement (Fig. 3). The resulting landscape is characterized by narrow sierras overlying roughly

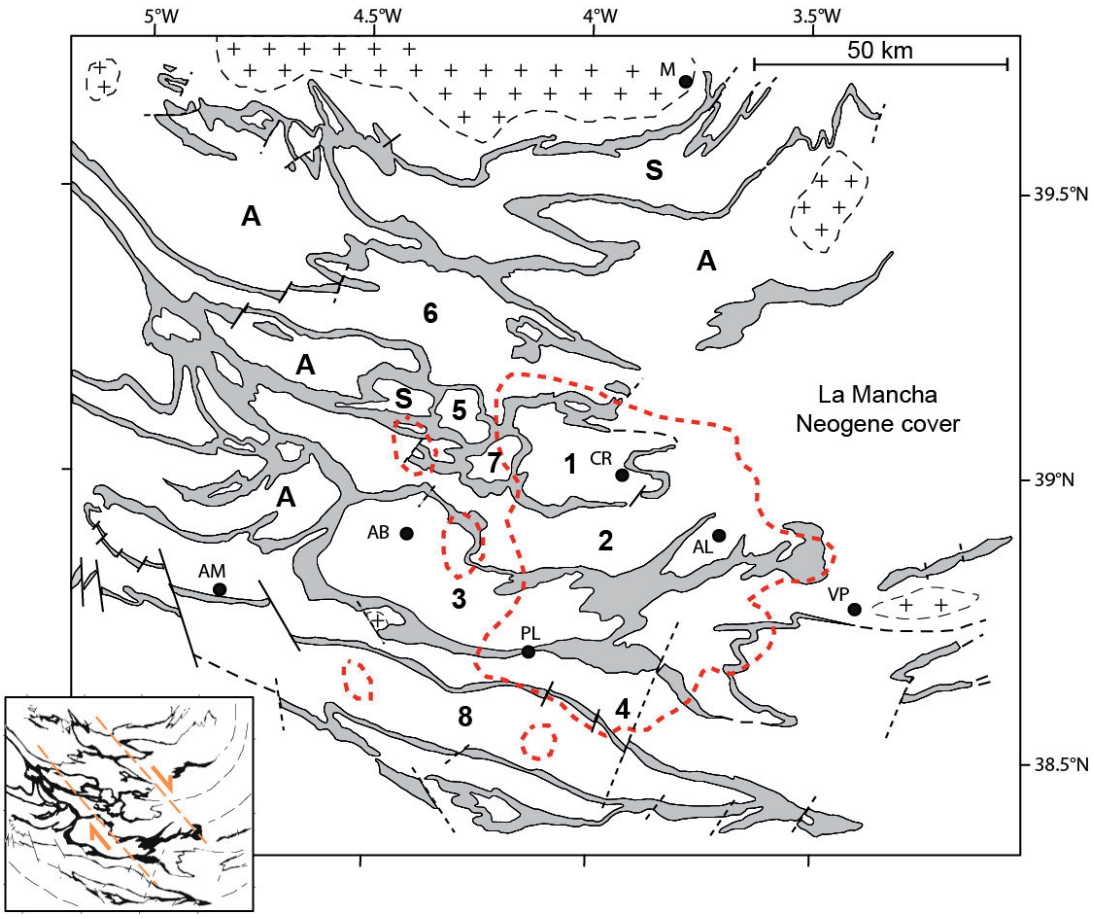

Fig. 3.- Location of the main Calatrava volcanic field and isolated centers (limited by red dashed lines; adapted from Ancochea *et al.*, 2004; Cebriá *et al.*, 2011; Sentre Domingo *et al.*, 2014) with respect to the Variscan structure (grey areas), as shown by the shape of the Lower Ordovician, erosion-resistant Armorican quartzite level. See location in Figure 2. Blurred granitic outcrops are shown by a cross pattern. Note the existence of an oblique, NW-directed, band of deformation in the central region of the map containing small and rounded folds, attributable to a right-lateral Variscan shear zone. A= anticline. S= syncline. 1= Ciudad Real Anticline. 2= Corral Syncline, 3 = Argamasilla Anticline. 4= Almadén-Puertollano Syncline. 5= Bullaquejo Anticline. 6= Guadarranque Syncline. 7= Porzuna Syncline. 8= Alcudia Anticline. M= Mora. CR= Ciudad Real. AL= Almagro. VP= Valdepeñas. PL= Puertollano. AM= Almadén. AB= Abenojar. The inset map shows the NW-directed right-lateral Variscan shear zone (orange lines) and the regional arc which modify the trends of the axial fold traces from N−S to the east to NW−SE to the west.

flat areas developed in the core of the km-sized folds, which are occasionally filled with epidermal, Neogene to Quaternary alluvial and lacustrine sediments. Sedimentary deposits reach locally a maximum of 550 m of thickness, but thickness is on average between 50 and 150 m increasing eastwards to the LMB (Sánchez Vizcaino, 2008). Regionally, the folds describe an arc, which modifies the trends of the axial traces from N−S in the east to NW−SE in the west. Moreover, there is an oblique, NW-directed band of more intense deformation characterized by rounded and smaller folds which disturb the main paired folds (Fig. 3). This oblique band is attributable to a deep-seated Variscan shear zone, whose right-lateral motion may contribute to compensate shortening in the intrados of the arc, as is documented by local contraction structures in the flanks of the northern folds (Fig. 3). The CVP seems to concentrate in an area which comprises the Ciudad-Real Anticline, the Corral Syncline as well as the eastern parts of the Abenojar-Argamasilla Anticline and the Almadén-Puertollano Syncline, in close relationship with the oblique Variscan shear zone. The CIZ is bounded to the south by the Badajoz-Cordoba Shear Zone (Burg *et al.,* 1981), latter redefined as the Central Unit (CU in Fig. 2; Azor *et al.,* 1994), which is a NW−SE-trending 5 km-wide band of high-grade metamorphics with slices of mafic rocks.

The Alpine intraplate deformation of the Iberian Massif has been ascribed to crustal-scale buckling processes on the basis of numerical and analogue modeling (Cloetingh *et al.*, 2002; Muñoz-Martín *et al.*, 2010; Fernández-Lozano *et al.*, 2012). This intraplate deformation has resulted from the N−S-directed convergence of Africa and Eurasia during Eocene-Oligocene times and is responsible for the main topographic features in the Variscan basement of the Iberian Peninsula (De Vicente and Vegas, 2009). In the central-southern part of the Iberian Massif, these main geomorphic features correspond to two basement uplifts or ridges (Toledo Mountains and Sierra Morena) separated by a zone of relative low relief which is drained by the Guadiana River (Fig. 2). In this intermediate low-relief area, the regional topography shows a

sort of NE-directed basement swell interfering with the E−W-trending Paleogene uplifts of the Toledo Mountains and the Sierra Morena. This interference of crustal-scale, E−W and NE−SW buckling folds is clearly evidenced by the outstanding heights of Sierra de la Calderina and Sierra Madrona (SC and SM respectively in Fig. 2). We assume that this later episode of intraplate deformation has its origin in the NW-directed Africa-Iberia convergence, which started in the Late Miocene and persists until Present-day (Rosenbaum *et al.*, 2002; Muñoz-Martín *et al.*, 2012). In this context, efficient stress transmission from the Prebetic front (PBF in Fig. 2), the external fold-and-thrust belt of the Betics, causes attendant buckling of the Variscan basement in the CVP (Vegas and Rincón-Calero, 1996).

In the area of the Iberian Massif corresponding to the CVP, the southern part of the CIZ including the CU, the structure of the crust has been investigated by means of two deep seismic reflection profiles: the ALACUDIA normal-incidence profile (ALCUDIA-NI in Fig. 2; Martínez Poyatos *et al.*, 2012; Simancas *et al.*, 2013; Ehsan *et al.*, 2014) and the ALCUDIA wide-angle profile (ALCUDIA-WA in Fig. 2; Ehsan *et al.*, 2015). The ALCUDIA-NI profile provides a detailed image of the Variscan crustal structures and significant differences between a weakly reflective upper crust and a thick, highly reflective and laminated lower crust. The P-wave velocity model derived from ALCUDIA-WA profile shows an upper-lower crust boundary located at 12 km of depth in the southernmost CIZ that deepens progressively up to 19 km at the Toledo Mountains. This velocity model also shows a progressive northward deepening of the Moho which is located at 31 km of depth in the southernmost CIZ and CU and becomes progressively deeper up to 34 km in the Toledo Mountains. 1D-averaged shear velocity modeling suggests that upper-lower crust boundary is located to 13 km of depth and the lithosphere-asthenosphere boundary (LAB) is located at ≈85 km in the Iberian Massif (Fig. 4; Palomeras *et al.*, 2014). These authors also refer to a local decrease in the LAB's depth, up to 65 km, in an E-W-trending band southwards of the CVP. The CVP has also been studied from 2D gravity modeling although not constrained by seismic data. Bergamín and Carbó (1986) suggested a lithosphere thinning beneath the CVP giving depths of 80-90 km for the LAB. These latter authors, as well as Sentre Domingo *et al.* (2014), proposed the existence of an anomalous density block in the mantle below the CVP with 4-6 km of thickness that was interpreted as a remnant of the volcanic activity.

3. Data and Methods

In the CVP and its vicinity, there is a dense coverage of gravity data provided by the Instituto Geográfico Nacional (IGN), the Empresa Nacional de Residuos Radioactivos (ENRESA), the Instituto Geológico y Minero (IGME) and the Universidad Complutense de Madrid (UCM) (Mezcua *et al.*, 1996; Álvarez García, 2002; Ayala, 2013; Fig. 5). Data reduction includes leveling to the absolute gravity network (IGN), instrumental drift and earth tide corrections. Free air, Bouguer plate and terrain corrections were calculated on the basis of the Geodetic Reference System of 1967 (GRS67) using a reduction density of 2.67 g/cm^3. The terrain correction was computed up to a radius of 166.7 km from the gravity station using two Digital Elevation Models (DEM): GTOPO30 (https://lta.cr.usgs.gov/GTOPO30) and SRTM90 (http://www2.jpl.nasa.gov/srtm). GTOPO30 data were used for a regional model gridded to intervals of 4000 m and SRTM90 data for a local model gridded to intervals of 500 m. Complete Bouguer anomaly data were interpolated to a regular grid of 5 km to avoid artifacts yielded by the irregular distribution of data. This grid size is large enough to characterize the wavelengths of the gravity anomalies caused by the deep sources modeled in the present study (>20 km).

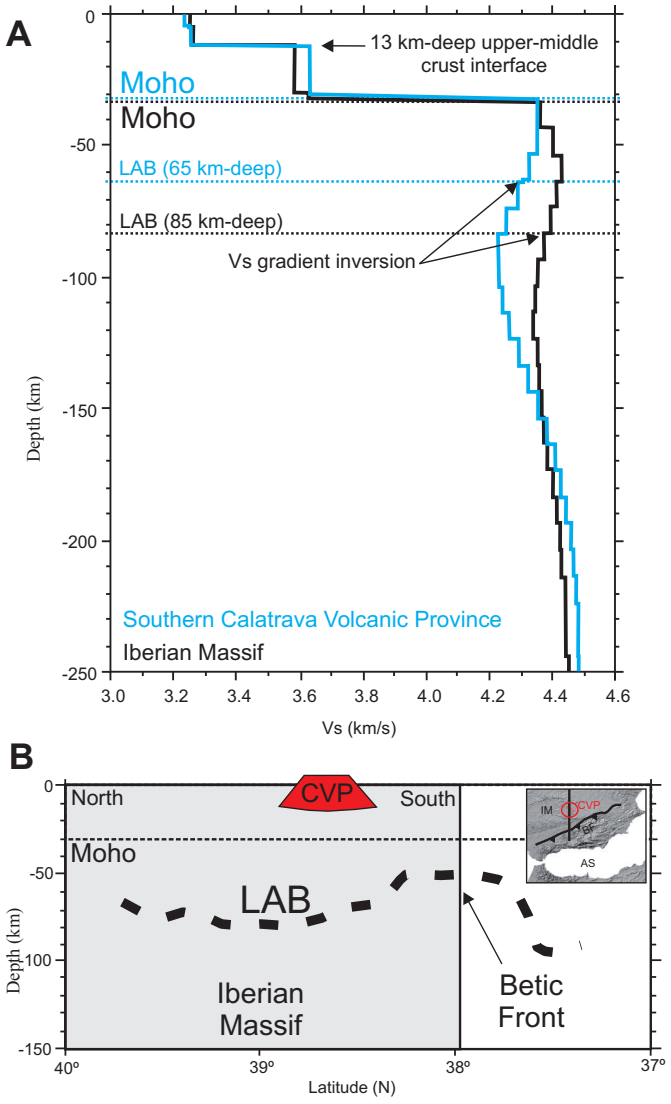

Fig. 4.- **A)** 1D-averaged shear velocity model for the Iberian Massif (black solid line) and for the CVP (blue solid line) modified from Palomeras *et al.* (2014). **B)** N−S-oriented absolute Vs cross-section through the CVP (modified from Palomeras *et al.*, 2014). See location in the inset map (IM= Iberian Massif. BF= Betic Front. AS= Alboran Sea). The grey zone shows the Iberian Massif. The red cone represents the position of the CVP.

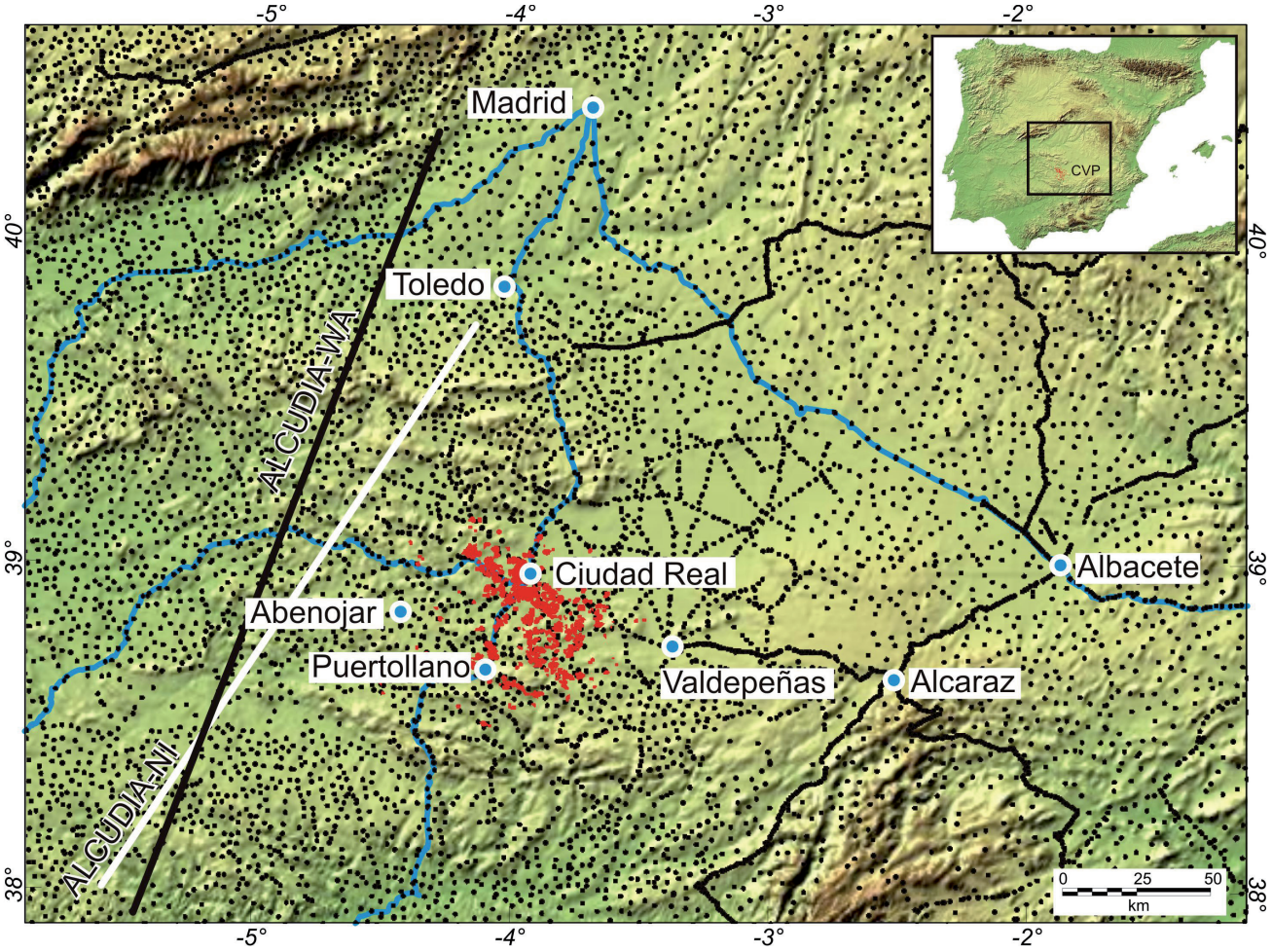

Fig. 5.- Digital elevation model (SRTM90) showing the study area, the location of the gravity stations (black dots) and the ALCUDIA deep seismic reflection transects: ALCUDIA normal incidence (ALCUDIA-NI) and ALCUDIA wide-angle (ALCUDIA-WA) (see the inset map for location; CVP= Calatrava Volcanic Province). Blue lines mark the main roads. Red-colored zones show the volcanic outcrops as in Figure 2.

Spectral analysis is a technique widely used in gravity analysis to design filters that make it possible to obtain regional trends and eliminate short wavelength signals produced by shallow sources. Upward continuation is one of the most effective filtering techniques for potential field maps in the frequency domain (Jacobsen, 1987; Blakely, 1995). This transformation attenuates anomalies with respect to wavelength; the shorter the wavelength, the greater the attenuation. Therefore, upward continuation tends to accentuate anomalies caused by deep sources at the expense of anomalies caused by shallow sources. Upward continuation does not provide direct information about the causative sources, but allows us to determine the amplitude and the wavelength of the regional gravity anomalies assuming relatively deep causative sources (e. g., Martos *et al.*, 2014). Because there is no seismic information about the crust in the CVP, we use the upward continuation transformation of the complete Bouguer anomaly to suppress or attenuate the short wavelength anomalies caused by shallower sources located in the crust (*c.f.*, Sentre Domingo *et al.*, 2014).

In order to aid 2+1/2D gravity modeling, we carried out a 2D-averaged spectral analysis (Spector and Grant, 1970) of the complete Bouguer anomaly and the upward continuation at different elevations to estimate the approximate depths of the main interfaces to be modeled and obtain a regional Bouguer anomaly map. Finally, six 2+1/2D gravity models were built using the regional Bouguer anomaly map. These models were extended far enough (>150 km) at both ends of the gravity profiles in order to avoid edge effects. Calculations of the gravity model response are based on the methods of Talwani *et al.* (1959) and Talwani and Heirtzler (1964) and the algorithms described in Won and Bevis (1987). The upward continued Bouguer anomaly (*i.e.*, regional Bouguer anomaly) has been shown as appropriate to model the Moho and LAB interfaces characterized by larger wavelengths (Martos *et al.*, 2014).

4. Results

4.1. Complete Bouguer anomaly map

The complete Bouguer anomaly map at the ground surface in the study zone (Fig. 6A) shows the different gravity signatures of each zone of the Iberian Massif (CU, Central Unit;

CIZ, Central Iberian Zone) and the surrounding areas such as the Betic Front (BF), the Spanish Central System (SCS), La Mancha Basin (LMB), the Iberian Chain (IC) and the Tagus Basin (TB). While the high density igneous areas are characterized by maxima, low density sedimentary areas reveal minima. This map shows a regional NW−SE-trending gradient from the region of the CU to the region of the IC and TB (Fig. 6A). Absolute minimum values are ≈-126 mGal in the TB and the IC, intermediate values are between -60 to -20 mGal in the CIZ, and there are absolute maximum values of 25 mGal in the CU. This regional gradient has been interpreted as indicative of an increase of the crustal thickness to the north as suggests the P-wave velocity model (Ehsan *et al.,* 2015). Main structural boundaries are marked by local highly-continuous gradients (black dashed lines in Fig. 6A): boundary between the SCS and the TB, boundary between the IC and the BF and boundaries between the Pedroches batholith (PB) and the CU and CIZ. Note the curved gradient in map-view (white dashed line in Fig. 6A) roughly marking the boundary between the outcrops of the CIZ with higher density values relative to the lower density values where the outcrops of the sedimentary rocks (*e.g.*, BF, TB and LMB) and acidic plutonic rocks are dominant (*e.g.*, SCS).

The CVP is located in the eastern region of the Iberian Massif, with intermediate values between -60 and -40 mGal (Figs. 6A and B). These intermediate values mark a relative minimum zone in the CIZ surrounded by a continuous gradient (sinuous white dashed lines in Fig. 6B). This gradient marks the boundary between the zones where the outcrops of the igneous and metamorphic rocks are dominant, forming the reliefs of Sierra de la Calderina and Sierra Madrona, and the zones where the thin sedimentary deposits of the LMB partially bury the Variscan basement rocks. The difference between this relative minimum zone and the relative maxima zones bordering the CVP reaches ≈ 16 mGal (Profile 1-1' in Fig. 6B). In the relative minimum zone, there are several isolated minimums (M1 through M5 in Fig. 6B) with values between -55 and -65 mGal that could be associated with localized depocenters of the sedimentary materials (Sánchez Vizcaino, 2008) or more probably hidden acidic plutonic domes (García-Lobón *et al.*, 2014). The minimum M5 corresponds to the outcrop of granitic rocks eastward of Valdepeñas (VP in Fig. 3). The volcanic centers are concentrated in an elongated NNW−SSE-trending threshold between these isolated minima (white line with arrowed ends in Fig. 6B). Petrophysical data showed that the volcanic rocks of the CVP are the densest rocks in the region with an average density of 2.96 g/cm^3 (García-Lobón *et al.*, 2014). Although volcanic rocks show a large outcrop zone in map-view, they probably represent a small volume because there are no distinguishable relative maxima in the complete Bouguer anomaly map related to the main volcanic outcrops. However, these higher densities of the volcanic rocks could contribute in part to the existence of this NNW−SSE-trending threshold of relative maxima because there is a spatial coincidence (profile 2-2' in Fig. 6B).

4.2 Spectral analysis of the Bouguer anomaly map

From the complete Bouguer anomaly map at the ground surface, we carried out successive filtering by upward continuation calculations to elevations of 10, 20, 30 and 40 km (Figs. 7A-D). All upward continued maps show the regional NW−SE-trending gradient also observed in the complete Bouguer anomaly map (*c.f.*, Fig. 6A). The higher the elevations of the upward continuation, the more attenuated are the local gradients and the relative maxima and minima associated to shallower causative bodies. Visual analysis of the regional Bouguer anomaly maps allows us to observe that in the upward continued map to 10 km there are still shorter wavelengths caused by shallower sources (Fig. 7A), but this attenuation is almost complete in the upward continued map to 20 km (Fig. 7B). Successive upward continuations over 20 km do not show significant differences because the shallower source effects have been completely removed (Figs. 7C and D). It should be noted that the relative minimum zone in the CVP is slightly attenuated in the upward continued map to 10 km and is still identifiable to 20 km, but it disappears with upward continuation transformations to higher elevations.

4.3 2D-averaged power spectrum

With a view to contributing to the identification and characterization of the anomaly wavelengths associated with the main sources modeled in the present study (*i.e.*, Moho and LAB), we calculated the 2D-averaged power spectrum of the complete Bouguer anomaly and of the upward continuations to different elevations (Fig. 8). The spectrum of the complete Bouguer anomaly and upward continuations to 10 and 20 km show the existence of significant signal concentrated in wavelengths of 48, 64, and 150 km. The spectrum of the complete Bouguer anomaly also shows the existence of signal concentrated in wavelengths of 24 and 32 km (inset in Fig. 8). The upward continuation to 10 km still shows a small signal concentrated in wavelengths of 32 km that is almost unidentifiable in the spectrums of the upward continuations to higher elevations. The spectrums of the upward continuation to elevations higher than 20 km do not show the existence of distinct dominant wavelengths below 100 km.

In order to avoid modeling signals with shorter wavelengths present in the complete Bouguer anomaly and in the upward continuation to 10 km, we use the upward continuation to 20 km as the regional Bouguer anomaly grid to perform the 2+1/2D gravity modeling of the lithospheric structure. Since the results of the 2D-averaged spectrum depend on several variables (*e.g.*, 2D anisotropy of the waveform, sampling rate and grid interval), we should interpret these wavelength values in a generic way to infer the depths of the main interfaces to be modeled (Spector and Grant, 1970; Martos *et al.*, 2014). Thus, wavelengths below 80 km should correspond with density variations in intra-crustal interfaces and the Moho (located at an average depth of 32-33 km, Ehsan *et al.*, 2015),

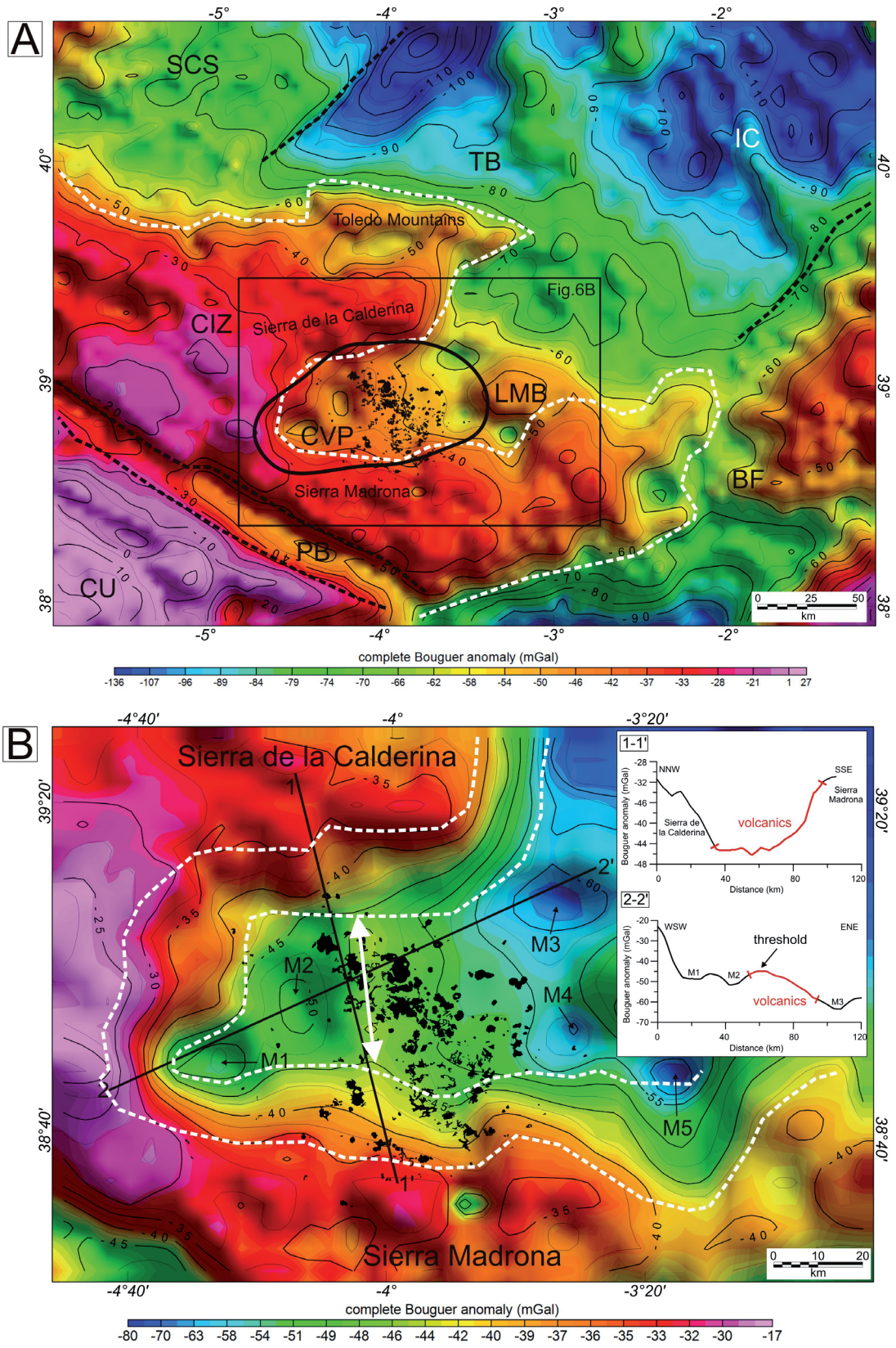

Fig. 6.- **A)** Complete Bouguer anomaly map. White dashed line marks a gravity gradient roughly bounding the external outcrops of the CIZ. Black dashed lines mark significant gradients bounding main structural zones. Black-filled zones show the volcanic outcrops. The black solid line shows the location of the subcrustal anomalous density block derived from the density modeling and described in Section 4.4. The inset shows the location of Figure 6B. SCS= Spanish Central System. CU=Central Unit. CIZ= Central Iberian Zone. TB= Tagus basin. LMB= La Mancha basin. CVP= Calatrava volcanic province. PB= Pedroches batholith. BF= Betic Front. IC= Iberian Chain. **B)** Enlarged sector of the complete Bouguer anomaly map of Figure 6A. White dashed lines outline the gradient between the CIZ outcrops (Sierra de la Calderina and Sierra Madrona) and the La Mancha basin (LMB) where the CVP is located. Black-filled zones show the volcanic outcrops. M1, M2, M3, M4 y M5 show the relative isolated minimum described in Section 4.1. Double-arrowed white solid line shows the NNW−SSE-trending threshold (relative maximum) described in Section 4.1. The inset shows two profiles of complete Bouguer anomaly crossing the CVP (see location in the map). The profile 1-1' shows the relative minimum at the CVP (red line) flanked by the relative maxima in the Sierra de la Calderina and the Sierra Madrona. The profile 2-2' shows the cross-section through the NNW−SSE-trending threshold (relative maximum) at the CVP related to the volcanic outcrops (red line)

and wavelengths above 100-120 km should correspond to causative sources located in the lithospheric mantle or in the LAB. This LAB has an average depth of 85 km in this area of the Iberian Massif in agreement with the Rayleigh wave tomography (Palomeras *et al.*, 2014).

4.4. 2+1/2D gravity modeling

We have selected six profiles from the upward continued complete Bouguer anomaly grid to 20 km (hereafter regional Bouguer anomaly) in order to carry out 2+1/2D gravity mod-

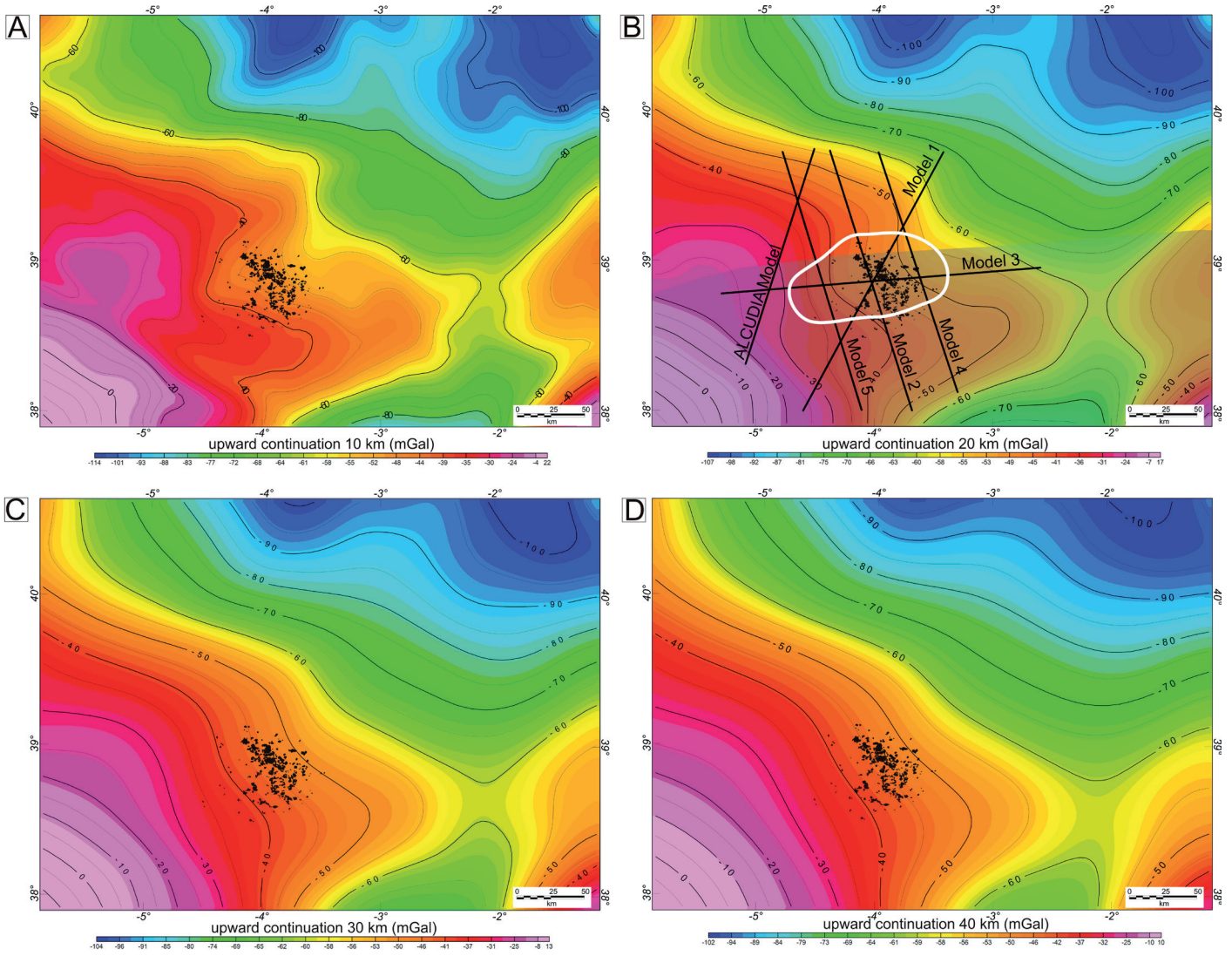

Fig. 7.- Regional Bouguer anomaly maps. Black-filled zones show the volcanic outcrops. **A)** Upward continuation to 10 km. **B)** Upward continuation to 20 km. Black solid lines mark the location of the 2+1/2D density models of Figures 9 and 10, and Appendixes A and B. The grey shaded area marks the northern zone of the thinned lithosphere zone suggested by Palomeras *et al.* (2014). The white solid line shows the extension of the sub-crustal anomalous density block derived from the density modeling of Section 4.4. **C)** Upward continuation to 30 km. **D)** Upward continuation to 40 km.

eling (Fig. 7B). The location and orientation of the profiles are determined in order to cross the main regional anomaly gradients and the location of the volcanic outcrops. The first model is located along the ALCUDIA-WA seismic transect (Ehsan *et al.,* 2015; Fig. 9) and is used as a template to model the geometry of the crust down to Moho. The seismic data allow us to constrain the depth and lateral geometry of the Moho and the intra-crustal layers. According to the reflectivity patterns of the ALCUDIA-NI seismic transect (Martínez Poyatos *et al.*, 2012) the crust was differentiated in upper, middle and lower layers, being mostly middle and lower crusts. According to the vertical velocity gradients of the ALCUDIA-WA seismic transect (Ehsan *et al.,* 2015), the crust was only differentiated in an upper and lower layers. The two-crustal layer model is coherent with the 1D-averaged shear velocity modeling for the Iberian Massif (Fig. 4A; Palomeras *et al.,* 2014). The crust along the ALCUDIA-NI and WA seismic transects has been previously modeled from complete Bouguer anomaly data (García-Lobón *et al.*, 2014; Ehsan *et al.,* 2015). Gravity models show the crust divided into three density layers or blocks: upper, middle and lower, being mostly middle and lower crusts. In the present study, to keep the coherency with previous gravity models, we reproduce the modeling using the same three crustal blocks (upper, middle and lower crustal layers) but from the signal of the regional Bouguer anomaly grid (*i.e.*, the upward continued complete Bouguer anomaly grid to 20 km). Averaged velocities and depths from seismic data models can be seen in Table 1 (Palomeras *et al.*, 2014; Ehsan *et al.,* 2015). Densities used for the gravity modeling of the crust have been inferred from the density-velocity semi-empirical relationships (Barton, 1986; Christensen and Mooney, 1995; Brocher, 2005; Table 1 and legend in Fig. 9) similar to those used by other authors in nearby areas (Palomeras *et al.*, 2011; García-Lobón *et al.*,

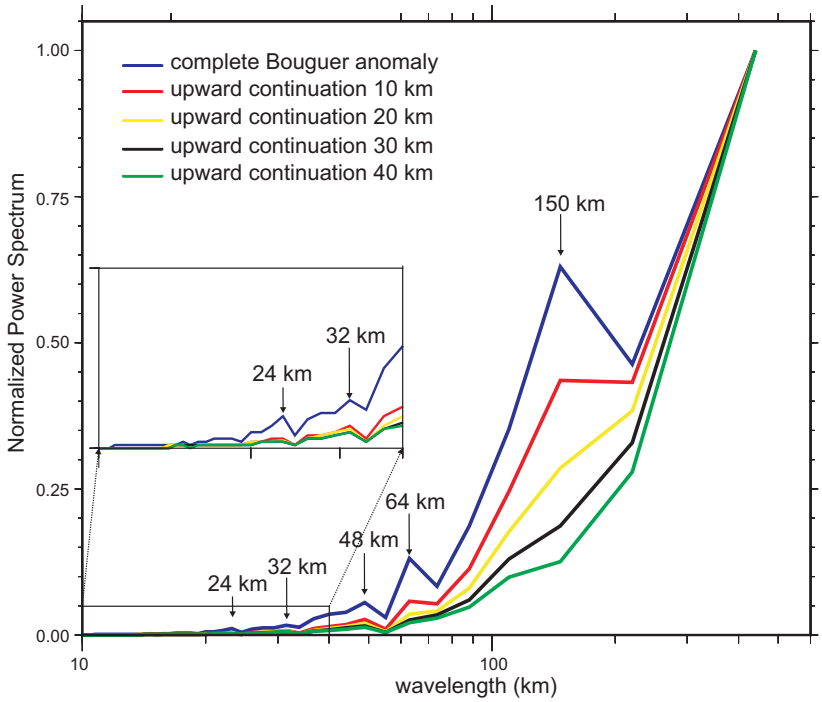

Fig. 8.- 2D-averaged power spectrum of the complete Bouguer anomaly and distinct upward continuations. Most significant wavelengths are indicated. The inset shows a vertical exaggerated sector (6.0x) of the wavelengths between 0 to 40 km.

Density block	Vp (km/s)	Vs (km/s)	Depth range (km)	Density (g/cm^3)
Upper crust	5.4-6.2	3.25	0 – 12-19	2.75
Middle crust	6.4	3.6	12-19 – 19-24	2.85
Lower crust	6.6-7.2	3.6	19-24 – 31-34	2.95
Lithospheric mantle	8.0	4.32 – 4.36 * 4.36 – 4.43 **	31-34 – 65 * 31-34 – 85 **	3.33
Asthenosphere		4.24 – 4.48 * 4.38 – 4.44 **	>65 * >85 **	3.3
Sub-crustal anomalous block			32 – 36	3.1

* Calatrava Volcanic Province.
** Iberian Massif.

Table 1.- Properties and depths used for the blocks in the adjusted gravity models. Vp values come from Ehsan *et al.* (2015). Vs values come from Palomeras *et al.* (2014).

2014; Ehsan *et al.,* 2015). In order to estimate the density of the lithospheric mantle and the asthenosphere, we used 1D-averaged shear velocity modeling for the Iberian Massif and for the CVP that is representative to a depth of 250 km (Fig. 4A; Palomeras *et al.*, 2014). This model is similar at crustal levels for the Iberian Massif and the CVP, showing two sharp gradients at 13 km and 32 km of depth corresponding with the base of the upper crust and the Moho respectively. From 40 to 150 km of depth, the 1D-averaged shear velocity models for the Iberian Massif and CVP diverge and show gradual Vs variations, though Vs is always higher in the Iberian Massif. Analyzing statically the Vs gradient inversion beneath the Moho, Palomeras *et al.* (2014) suggested that the LAB is located on average at a depth of ≈85 km in the Iberian Massif and at a depth of ≈65 km in the CVP (Fig. 4A). The 2D shear velocity model inferred from seismic tomography shows that the LAB is located on average at a depth of ≈85 km northward of the CVP (Fig. 4B). Beneath and southward of the CVP, the LAB becomes shallower to a depth of ≈65 km at the boundary between the Iberian Massif and the Betic Front (grey-shaded zone in Fig. 7B). Averaging the Vs values from the 1D-averaged shear velocity model (Vs=4.36 km/s for the lithospheric mantle and Vs=4.33 km/s for the asthenosphere) and using the Vs-Vp and density-Vp semi-empirical relationships (Barton, 1986; Christensen and Mooney, 1995; Brocher, 2005), we have assigned an average density of 3.33 g/cm^3 for the lithospheric mantle and 3.3 g/cm^3 for the asthenosphere (Table 1). Note that we used constant density values for the different crustal blocks because the ALCUDIA-WA seismic transect does not shows lateral velocity changes in the crust in our study zone (Ehsan *et al.*, 2015), and also because 1D-averaged shear velocity modeling does not provide enough detail to constrain any lateral changes of density in the lithospheric mantle and in the asthenosphere (Palomeras *et al.*, 2014).

ALCUDIA Gravity Model

The NE−SW-trending ALCUDIA Model is located to the west of the CVP and crosses transversally the NW−SE- to WNW−ESE-trending structures of the CIZ formed in the Variscan orogeny (Fig. 7B; Simancas *et al.,* 2013). The southern termination of this model reaches the boundary between the CIZ and the Ossa Morena Zone(OMZ) located along the NW−SE-trending Badajoz-Cordoba Shear Zone (Burg *et al.*, 1981), later redefined as the Central Unit (CU in Fig. 2; Azor *et al.*, 1994). The filtered observed Bouguer anomaly profile shows a regional gradient with an absolute maximum of -16 mGal at the southwestern end in the CU and an absolute min-

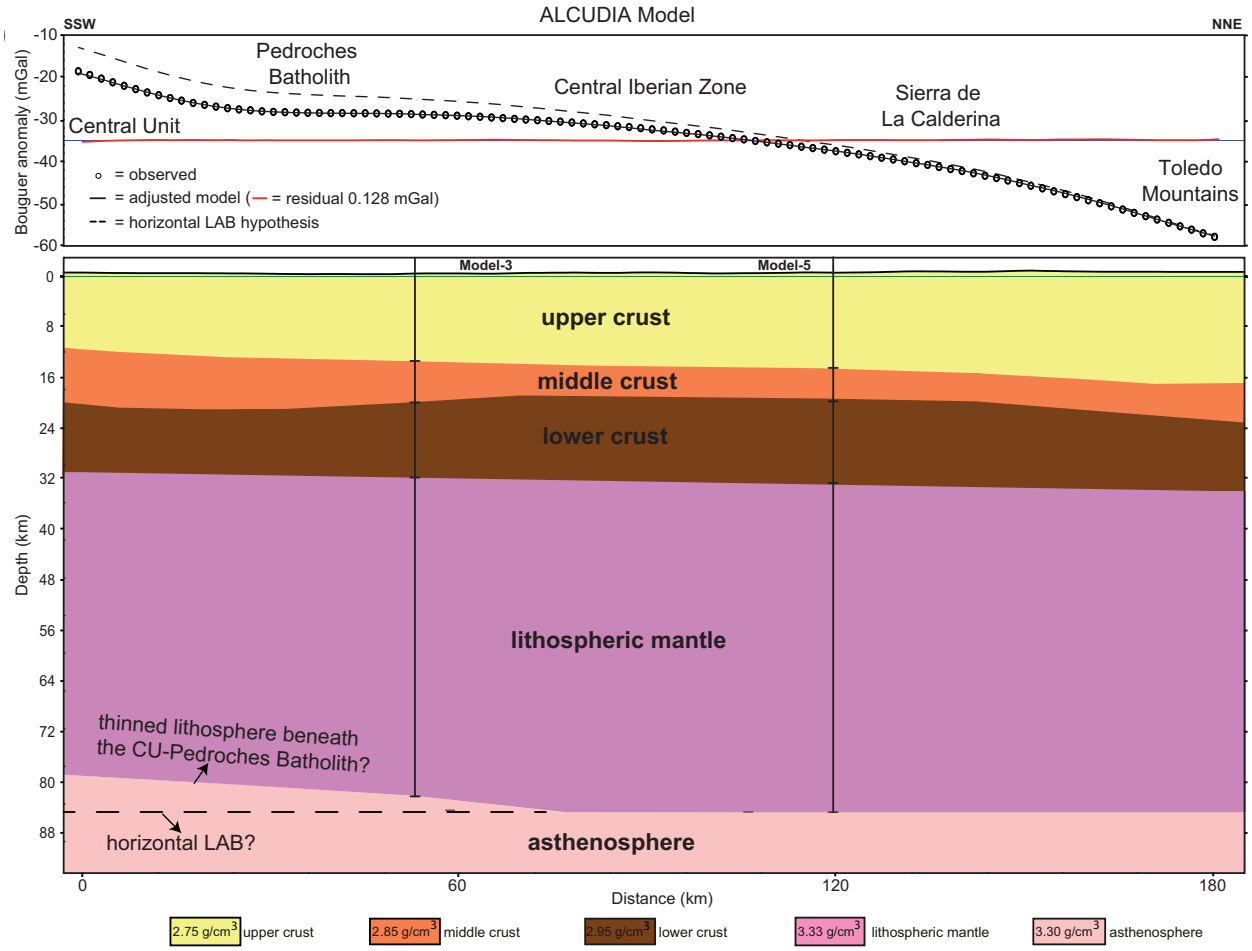

Fig. 9.- 2D gravity model performed along the ALCUDIA-WA seismic profile. See Location in Figure 7B. Top diagram: Black circles show the observed regional Bouguer anomaly. The black line shows the gravity response of the calculated model. Red line shows the residual (*i.e.*, difference between observed and calculated anomalies). Bottom diagram: Calculated models. See legend for interpretation of the colors and the density blocks. Densities are given in g/cm^3. Vertical lines show the intersection with other models of the present study shown in Figure 10. CU= Central Unit. LAB= Lithosphere-Astenosphere Boundary.

imum of -57 mGal at the northeastern end in the acidic rocks of the Toledo Mountains (top diagram in Fig. 9). The regional gradient shows a local smoothing over the Pedroches batholith, which is a NW−SE-trending formation of acidic plutonic rocks (*e.g.*, García-Lobón *et al.*, 2014). Northeastward, the gradient is uniform through the CIZ and becomes slightly steeper in the Sierra de la Calderina and Toledo Mountains.

The calculated model shows a Moho dipping uniformly ≈1º to the north (Fig. 9). The calculated depth of the Moho is 31 km in the southwestern end (*i.e.,* CU) and 34 km in the in the northeastern end (*i.e.,* Toledo Mountains) in agreement with P-wave velocity model (Ehsan *et al.*, 2015). The calculated LAB is located at a depth of 85 km with a horizontal geometry except at the southwestern end in the Pedroches batholith and in the CU, which progressively rises up to ≈80 km of depth in agreement with the lithospheric thinning proposed from the 1D-averaged shear velocity modeling (bottom diagram in Fig. 9; Palomeras *et al.*, 2014). The regional gradient is adjusted by means of: a smooth and uniform deepening of the upper-middle crustal interface and the Moho, and a thickening of the lower crust in the CIZ and in the Sierra de la Calderina. The depth of the upper-middle crustal interface varies uniformly from 12 km in the OMZ to 19 km in the Toledo Mountains. The depth of the middle-lower crustal interface varies from 19-21 km in the SW and NE terminations (*i.e.,* in the CU-Pedroches batholith and Toledo Mountains respectively) to 17-18 km in the center of the model (*i.e.,* in the CIZ and Sierra de la Calderina). The local smoothing of the gradient over the Pedroches batholith can be adjusted varying locally the geometry of the middle-lower crust interface in agreement with the P-wave velocity model (Ehsan *et al.,* 2015; Table 1). In order to test the sensitivity of the gravity modeling and to quantify the effect of the lithospheric thinning beneath the CU and the Pedroches batholith (thinned lithosphere in the bottom diagram of Fig. 9), we have modified the adjusted model building a horizontal LAB at 85 km of depth beneath the CU and the Pedroches batholith (horizontal LAB in the bottom diagram of Fig. 9). The gravity response is a progressive mass excess starting from the northern CIZ to the CU, where the misfit related to the observed data reaches a maximum amplitude of ≈5 mGal (black dashed line in the top diagram of Fig. 9). This mass ex-

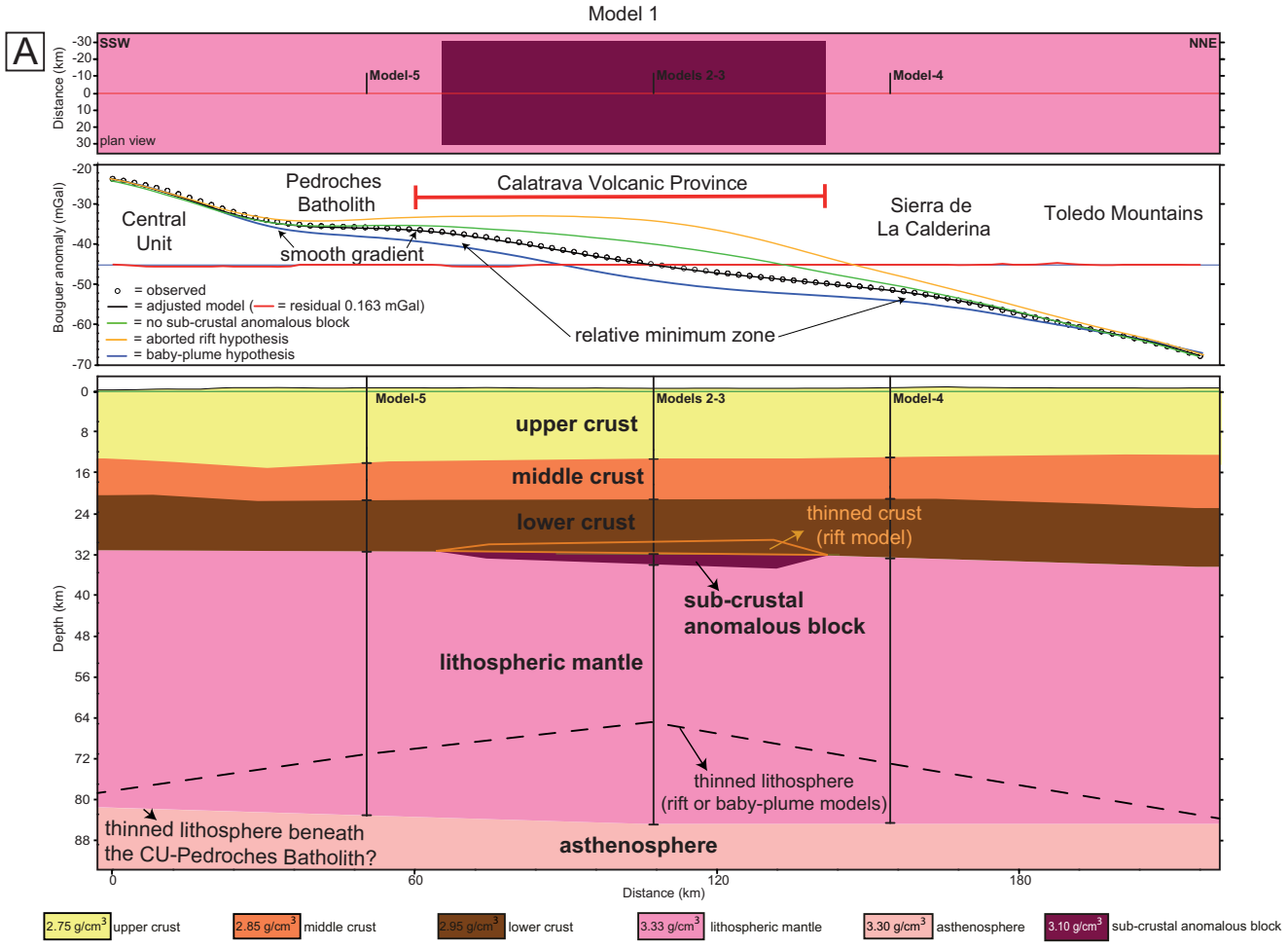

Fig. 10.- (this page and the next one) 2+1/2D gravity models along the profiles located in Figure 7B. Top diagram: Plan view for the modeling in 2+1/2D (plan view at Moho depth in the bottom diagram model) showing the position of the model (red solid line) and the lateral extension of the sub-crustal anomalous block. The intersections with other models are indicated. Middle diagram: Black circles show the observed regional Bouguer anomaly. The black solid line shows the gravity response of the calculated model. The red line shows the residual in mGal (*i.e.*, difference between observed and calculated anomalies). The green solid line shows the calculated gravimetric response of a model without a sub-crustal anomalous density block. The orange solid line shows the calculated gravimetric response of a model with thinned lithosphere beneath the Calatrava Volcanic Province (aborted rift hypothesis). The blue solid line shows the calculated gravimetric response of a model with a thinned lithospheric mantle beneath the Calatrava Volcanic Province (baby-plume hypothesis). The extension of the volcanic outcrops is indicated. Bottom diagram: Calculated models. See legend for interpretation of the colors and the density blocks. Densities are given in g/cm^3. The black dashed line shows the position of the LAB interface in the cases of a thinned lithosphere beneath the CVP. Orange solid line shows the anomalous density block built into the bottom of the lower crust assuming a thinned crust. Vertical lines show the intersection with other models of the present study. CU= Central Unit. LAB= Lithosphere-Astenosphere Boundary. A) Model 1 performed sub-parallel to the ALCUDIA-WA seismic profile across the CVP. B) (next page) Model 2. C) (next page) Model 3.

cess is yielded by the replacement beneath the southwestern end of the model of a relatively low-density asthenospheric mantle with a high-density lithospheric mantle. The slight steepening in the calculated regional gradient yielded by the horizontal LAB could be compensated changing slightly the geometry of the crustal interfaces between the depth ranges inferred from the seismic data (Ehsan *et al.*, 2015). Our gravity modeling, therefore, does not show enough sensitivity to test the existence of the lithospheric thinning (±10 km) in the CU-Pedroches batholith suggested from 1D-averaged shear velocity modeling (Palomeras *et al.*, 2014). However, because of the lack of other constraints, we adopted this geometry for the LAB to adjust the gravity models in the CVP.

Gravity Models in the Calatrava Volcanic Province

We have constructed five gravity models in the CVP and its vicinity (Fig. 10 and Apps. A and B). The models have distinct orientations (Fig. 7B) in order to test possible lateral changes in the lithospheric structure and considering the distinct orientations of the NW−SE- to WNW−ESE-trending Variscan and NE−SW-trending Alpine structures (*e.g.*, De Vicente *et al.*, 2008; Simancas *et al.*, 2013). All models are built using the ALCUDIA Model as the template for the crustal structure (Fig. 9) and the intersections among different models have been used to homogenize the structure of the modeled blocks (vertical lines in Figs. 9 and 10).

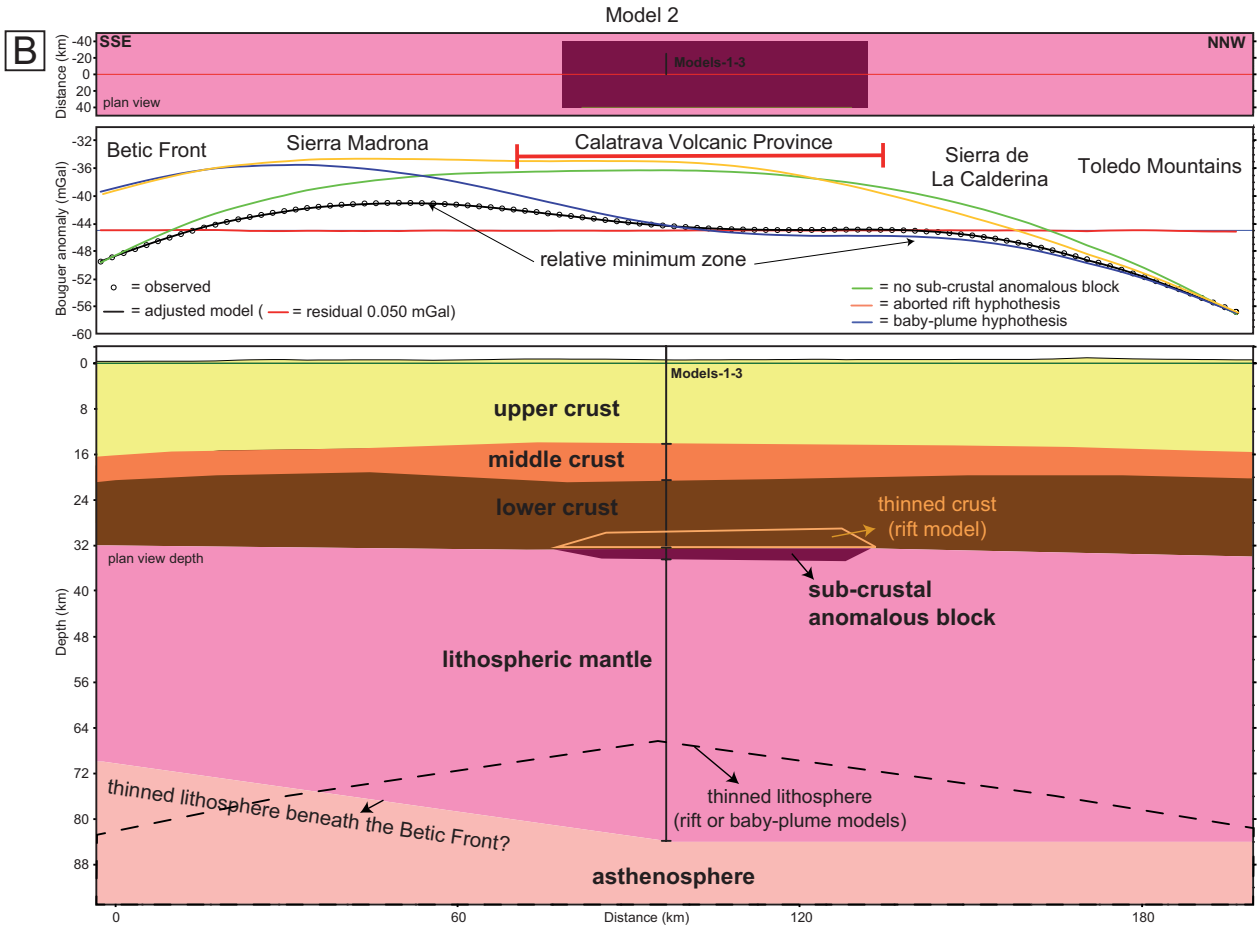
Model 2
B
SSE
NNW
Models-1-3
plan view
Distance (km)
Betic Front
Sierra Madrona
Calatrava Volcanic Province
Sierra de
La Calderina
Toledo Mountains
relative minimum zone
= observed
= adjusted model (= residual 0.050 mGal)
= no sub-crustal anomalous block
= aborted rift hyphothesis
= baby-plume hyphothesis
Bouguer anomaly (mGal)
upper crust
middle crust
lower crust
thinned crust
(rift model)
plan view depth
sub-crustal
anomalous block
lithospheric mantle
thinned lithosphere beneath the Betic Front?
thinned lithosphere
(rift or baby-plume models)
asthenosphere
Depth (km)
Distance (km)

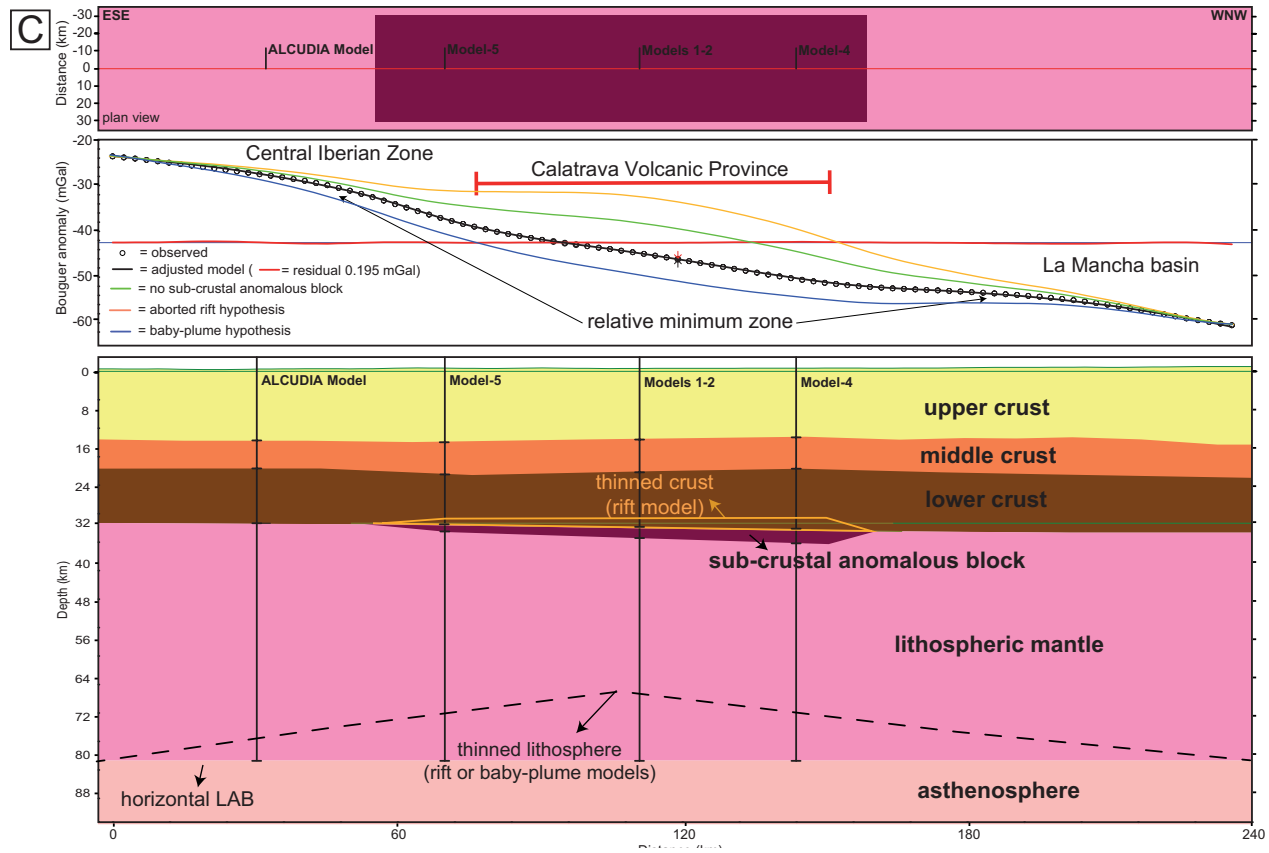
Model 3
C
ESE
WNW
ALCUDIA Model
Model-5
Models 1-2
Model-4
plan view
Distance (km)
Central Iberian Zone
Calatrava Volcanic Province
= observed
= adjusted model (= residual 0.195 mGal)
= no sub-crustal anomalous block
= aborted rift hypothesis
= baby-plume hypothesis
La Mancha basin
relative minimum zone
Bouguer anomaly (mGal)
upper crust
middle crust
lower crust
thinned crust
(rift model)
sub-crustal anomalous block
lithospheric mantle
thinned lithosphere
(rift or baby-plume models)
horizontal LAB
asthenosphere
Depth (km)

The NE−SW-trending Model 1 is sub-parallel to the ALCUDIA Model, but crosses the center of the CVP (Fig. 7B). The observed filtered Bouguer anomaly profile shows a regional gradient similar to the ALCUDIA Model, with an absolute maximum of -23 mGal localized over the CU and an absolute minimum of -68 mGal localized in the acidic rocks of the Toledo Mountains (middle diagram in Fig. 10A). There is a local smoothing of the observed gradient in the Pedroches batholith and a local relative minimum zone in the CVP. This relative minimum zone does not exist in the ALCUDIA Model (Fig. 9), and has a wavelength of ≈100 km and maximum amplitude of ≈5 mGal relative to the trend of the observed regional gradient. The NW−SE-trending Models 2, 4 and 5 are parallel to each other and cross the CVP in the central, eastern and western zones respectively (Fig. 10B; Apps. A and B). Observed filtered anomaly profiles cross transversally the regional gradient that roughly separates the igneous outcrops of the CIZ from the thin sediment deposits of La Mancha Basin where the CVP is located (Fig. 6B). These anomaly profiles show an M-shaped waveform characterized by two regional minima in the ends flanking a broad zone of maxima that in turn has a local relative minimum in the center (*i.e.*, a succession of minima and maxima). The absolute minima are located at the northwestern end in the Toledo Mountains, with values on average of ≈-55 mGal, and vary at the southeastern end from ≈-55 mGal in the Betic Front (App. A) to ≈-35 mGal in the Pedroches batholith (App. B). The local relative minimum centered in the CVP has a wavelength of ≈90 km and a maximum amplitude of ≈4 mGal relative to the flanking maxima located in the Sierra Madrona and the Sierra de la Calderina. The WSW−ENE-trending Model 3 crosses the center of the CVP and extends eastward over the La Mancha Basin (Fig. 10C). The observed anomaly profile shows a regional gradient with an absolute maximum of -23 mGal localized in the CIZ and an absolute minimum of -60 mGal localized in the La Mancha Basin. There is a relative minimum zone in the CVP with a wavelength of ≈150 km and maximum amplitude of ≈5 mGal relative to the trend of the regional gradient.

As in the case of the ALCUDIA Model, we built Models 1 through 5 with a smooth northward dipping geometry of the Moho having depths of 31 km in the southern end and 34 km in the northern end. The LAB has a horizontal geometry at 85 km of depth, with a progressive lithosphere thinning up to ≈70 km beneath the BF and CU (Fig. 10B; Apps. A and B). However, in contrast to the ALCUDIA Model (Fig. 9), Models 1 through 5 show a mass excess localized over the relative minimum zone in the CVP (green line in Fig. 10). To adjust the models in the relative minimum zone centered in the CVP, it is necessary to add a low-density or anomalous density block with tabular geometry located at the base of the lower crust beneath the CVP (sub-crustal anomalous block in Fig. 10). This new block has intermediate densities between the 2.95 g/cm^3 of the lower crust and the 3.33 g/cm^3 of the lithospheric mantle. We have assigned a density of 3.1 g/cm^3 for this block, but we have tested densities between 3.05 y 3.15 g/cm^3, yielding similar gravity responses. The geometry, position and anomalous density of this block yield enough mass deficit related to the surrounding lithospheric mantle material to adjust the model in the CVP (black solid line in Fig. 10). Integrating the information from Models 1 through 5, we observe that this block disappears away from the CVP because it is strongly dependent on the existence of the relative minimum zone centered in the CVP (Fig. 6B). The limited extension of this block to the CVP is well observed in Model 3 (Fig. 10C), which allows us to observe that the block does not continue eastward to the La Mancha Basin. 2+1/2D gravity modeling made it possible to laterally truncate the sub-crustal anomalous block in agreement with the extension observed in Models 1 through 5 (top diagrams in Fig. 10). Then, integrating the information of Models 1 through 5, we have determined in an approximate way the extension of the sub-crustal anomalous density block (white encircled zone in Fig. 7B). This block shows an elliptical shape in map-view with a WSW-ENE-trending semi-major axis reaching 110 km of length and a NNW−SSE-trending semi-minor axis with 65 km of length (Fig. 11). The average thickness is between 2 and 3 km, with a local maximum of 3.4 km in the eastern zone. In general, the location of the volcanic outcrops coincides with the center of the block but there is a higher concentration of volcanic outcrops in the eastern zone where the block is lightly thicker.

5. Discussion

5.1. Insights from gravity modeling

Gravity modeling always provides a non-unique solution, but it is a useful tool to reject a model if it is totally unable to fit the data (*e.g.*, Blakely, 1995). For instance, that is the case if we try to build a gravity model throughout the CVP without including a sub-crustal anomalous density block beneath the volcanic outcrops. We have built a series of adjusted models that are reasonable and realistic from a geological and physical viewpoint (Fig. 12A), but it is necessary to explore alternative hypotheses and geodynamic scenarios (Figs. 12B and C). For that, we have used the geometry of the density blocks of the adjusted models in those zones better constrained with seismic data and have varied the geometry of the rest to analyze the distinct gravity responses.

Sub-crustal anomalous block

Our models in the CVP show a good fit with a crust having an almost constant thickness with the Moho located between 31 and 34 km of depth in agreement with seismic data (Ehsan *et al.,* 2015). If there is any flexural geometry in the Moho, it must be very smooth and with a wavelength exceeding 200 km, because it cannot be properly detected with either seismic or gravity modeling. On the other hand, it would also be possible to adjust the NW−SE-trending models (2, 4 and 5) in

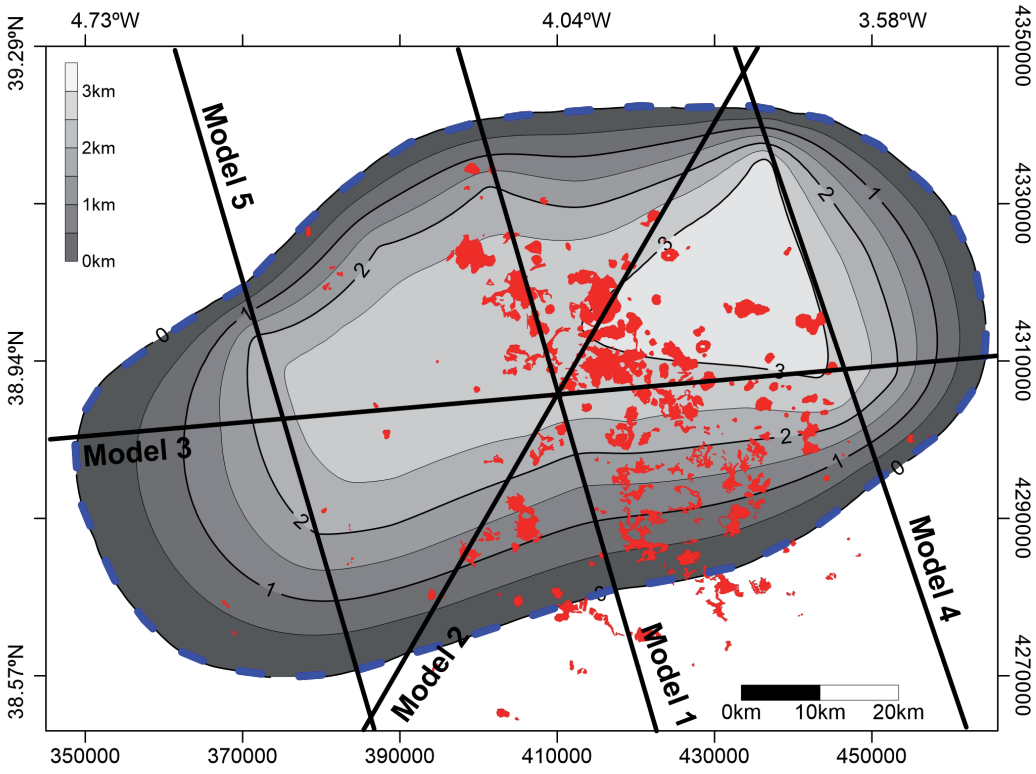

Fig. 11.- Contoured map showing the calculated extension and thickness of the sub-crustal anomalous density block. Contour interval is 0.5 km. Red-filled zones show the volcanic outcrops. Solid black lines show the location of the gravity models.

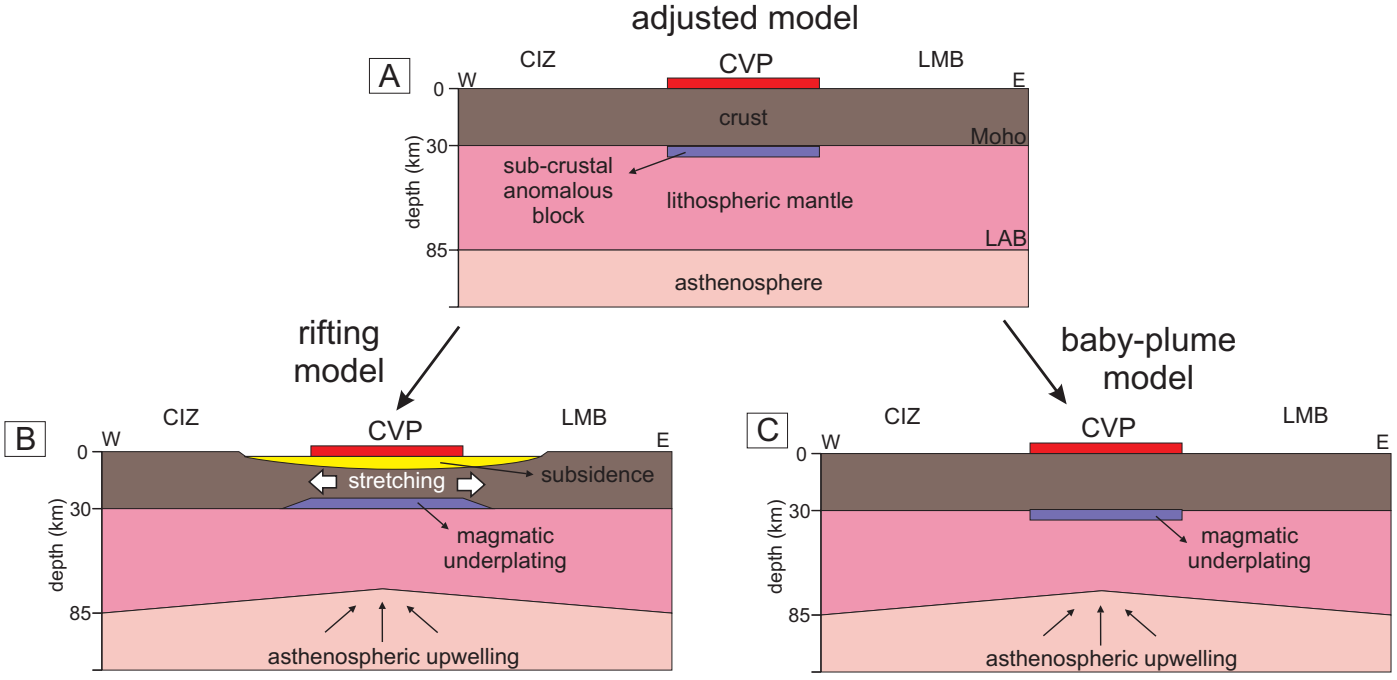

Fig. 12.- E−W-oriented cross-sections showing alternative scenarios for the lithosphere structure beneath the CVP. **A)** Model compatible with the gravity model of this study: sub-crustal anomalous block beneath CVP and horizontal LAB. The local decrease of the pressure beneath the lithosphere in the CVP because of the lithospheric folding (undetectable from our gravity modeling) is likely to bring on basaltic magmatism along and below the swell in the Calatrava region (*c.f.*, Shin *et al.*, 2012). **B)** Aborted rifting hypothesis (Cebriá, 1992; López-Ruiz *et al.*, 1993). Lithosphere (crust + lithospheric mantle) thinning beneath the CVP. The horizontal stretching of the lithosphere yields subsidence in the upper crust with the formation of a thick continental rift basin, and magmatic underplating into the lower crust. There is magmatic underplating into the "void" space generated into the lower crust. **C)** Baby-plume hypothesis (Humphreys *et al.*, 2010). Lithosphere thinning beneath the CVP, but no crustal thinning. The volcanism is yielded by a hot finger detached from an active megaplume below the Canary and Azores Islands and the western Mediterranean Sea (Stoppa *et al.*, 2011). There is magmatic underplating beneath the lower crust.

a similar way by building a very smooth ENE-WSW-oriented crustal antiform (with a hinge zone centered on the CVP), though we have no constraints in this case. Independently of an almost flat or very gently-folded Moho geometry, all models need the existence of a sub-crustal anomalous low-density block with tabular-like geometry beneath the CVP. This block allows a good fit of the relative minimum zone of the regional Bouguer anomaly located in the CVP with a wavelength of ≈100 km. If we use the same geometry of the adjusted model, but replace this block (3.10 g / cm^3) with lithospheric mantle (3.33 g / cm^3), the gravimetric response is a mass excess in relation to the observed data localized over the relative minimum centered in the CVP (green solid line in Figs. 10A-C). The presence of the lithospheric mantle just below the lower crust generates a misfit with a wavelength of 140-150 km and maximum amplitude of ≈4-6 mGal relative to the observed data (Figs. 10A-C).

The localization of this anomalous block at sub-crustal depths can also be approached in an approximate way from the analysis of the regional Bouguer anomaly maps since its existence is associated with the relative minimum zone in the CVP. Upward continued Bouguer anomaly maps to 10 and 20 km still show the relative minimum zone in the CVP that is fitted in the gravity models by the addition of the sub-crustal anomalous block (Figs. 7A and B). However, this relative minimum zone is not observable in upward continued Bouguer anomaly maps over 20 km (Figs. 7C and D), because the short wavelengths (<100 km) are removed by the upward continuation. This fact suggests that the causative sources of the relative minimum zone should be relatively deep, because the signal is still observed in the continued Bouguer anomaly map to 20 km. This map has significant signal concentrated in wavelengths of 48 and 64 km that could correspond with the lower crust and Moho depths (Fig. 8). On the other hand, such causative sources cannot be associated with the LAB because to modify this interface located at depths between 65 and 85 km yields a gravity response changing the regional gradient over wavelengths longer than 100 km (Figs. 9 and 10). Thus, the conjunction of these inferences suggests that the causative source of the relative minimum zone in the CVP should be located at least at Moho or sub-crustal depths, but much shallower than LAB depths.

Previous gravity modeling in the CVP, not constrained with seismic data, already suggested the existence of an anomalous density block in the upper mantle below the CVP with 6 km of maximum thickness (Bergamín and Carbó, 1986) or of 3 km of maximum thickness (Sentre Domingo *et al.*, 2014). Our gravity modeling corroborates the existence of such a sub-crustal body beneath the CVP with a maximum thickness of 3.4 km in agreement with previous modeling. With the integration of the information of Models 1 through 5 constrained with seismic data, we have improved the location and an extension sub-crustal block related to the volcanic outcrops (Fig. 11). We interpret this anomalous body as a result of the underplating of the magmatic materials beneath the crust. Since the ascending basaltic magmas from the LAB have a higher density than the crust, a significant part of the magma would have been underplated beneath the crust, and only a small portion of it intruded up to the shallow crust or erupted forming the CVP.

Rifting hypothesis

The intraplate volcanism that occurred in the CVP was explained adopting a model of an aborted rift yielded by a WSW-ESE-oriented extension (*e.g.*, Cebriá, 1992; López-Ruiz *et al.*, 1993). The horizontal stretching of the lithosphere is necessarily accompanied by a thinning of the lithospheric mantle and the crust (Fig. 12B; *e.g.*, Davis and Kusznir, 2004 and references therein). The thinning of the lithospheric mantle yields a "void" space at the bottom of the lithosphere to be occupied by relatively low-density asthenospheric material (*i.e.*, asthenospheric upwelling). The thinning of the crust yields a "void" space at the bottom of the crust to be occupied by relatively high-density mantelic material and at the top of the crust to be occupied by a structurally-controlled sedimentary basin (*i.e.*, continental rift basin). To test this geodynamic scenario, we built a gravity model with a lithospheric mantle thinning of 20 km (*i.e.*, from 85 km up to 65 km of depth) beneath the CVP in agreement with the maximum thinning suggested by 3D seismic tomography data for the region (*c.f.*, Palomeras *et al.*, 2014) (dashed black line in the bottom diagram of Fig. 10). To simulate the mantelic material occupying the "void" space generated in the bottom of the lower crust (2.95 g / cm^3), we have used the symmetric geometry of the same sub-crustal anomalous density block (3.1 g / cm^3), but built intruded into the bottom of the lower crust (orange block in the bottom diagram of Fig. 10). In agreement with the structural and shallow geophysical observations, we do not model a thick sedimentary basin because the sedimentary cover of the La Mancha Basin in the CVP is only epidermal, on average between 50 and 150 m in thickness (Sánchez Vizcaino, 2008). The gravity response is a generalized mass excess with maximum amplitude of ≈8-10 mGal in the CVP relative to the observed regional Bouguer anomaly (orange line in the middle diagram of Fig. 10). The mass excess is only produced by a high-density block in the lower crust, because on the contrary, the lithospheric thinning tends to yield mass deficit. Although the lithospheric mantle thinning generates a regional mass deficit, it does not compensate the local mass excess yielded by the existence of relatively high-density mantelic material intruded into the base of the lower crust beneath the CVP. Our gravity modeling therefore suggests the inexistence of a thinned lower crust in the CVP independently of the existence of a significant lithospheric thinning.

Baby-plume hypothesis

An alternative hypothesis to explain the intraplate volcanism that occurred in the CVP could be to adopt the existence of a small plume beneath the CVP (Humphreys *et al.*, 2010;

Fig. 12C). This mechanism was used to explain other small-volume intraplate volcanism in the European Cenozoic Volcanic Province in central Europe (*c.f.*, baby-plume, hot finger, finger plume; Lustrino and Carminati, 2007). This hypothesis consists of an asthenospheric upwelling that yields a lithospheric mantle thinning beneath the CVP. However, in contrast to the rifting hypothesis here there is no crustal thinning. We simulate this scenario from the adjusted model building a lithospheric mantle thinning up to 20 km (*i.e.*, from 85 km up to 65 km of depth) beneath the CVP in agreement with the maximum thinning suggested by 3D seismic tomography data for the region (*c.f.*, Palomeras *et al.*, 2014) (dashed black line in the bottom diagram of Fig. 10). The denser lithospheric mantle is replaced by the lighter asthenosphere yielding a mass deficit relative to the observed data with maximum amplitude of ≈4 mGal in the CVP (blue solid line in Fig. 10). The mass deficit extends to the Sierra de la Calderina and there is mass excess in the areas of the CU and the BF where the LAB geometry has changed from the adjusted model. The sub-crustal anomalous density block beneath the CVP yields a mass deficit with a wavelength of ≈100 km that is summed to the mass deficit of the thinned lithospheric mantle with wavelengths of >150 km. Thus, these two contributions to the mass deficit have different wavelengths controlled by the depth and density contrast of the causative sources. If we replace the sub-crustal anomalous block by lithospheric mantle, there is still a mass deficit with a wavelength of >150 km but with a maximum amplitude of ≈2-4 mGal in the CVP. Then, replacing the sub-crustal anomalous block does not compensate the mass deficit yielded by the thinned lithospheric mantle beneath the CVP. These observations suggest the inexistence of a significant lithospheric mantle thinning beneath the CVP since it yields a regional mass deficit that is not observed in the regional Bouguer anomaly. If there is a lithospheric thinning beneath the CVP, it should be small, below ≈10 km, and therefore outside the sensitivity of the gravity modeling. This observation is in agreement with the slope of the lithospheric folds in the continental crust of Iberia, which are very gentle: 1 – 2 km of amplitude for wavelength of about 250 km (Muñoz-Martín *et al.*, 2010). Such variations in the depth of the LAB are outside the sensitivity of our gravity modeling. However, we can reject the existence of a lithosphere thinning beneath the CVP larger than 10 km, as was suggested by Bergamín and Carbó (1986).

5.2 Geodynamic implications

The gravity models presented here show a crust with a very small northward thickening (between 31 and 34 km) that does not support the rifting model adopted for this intraplate volcanic province in previous papers (*e.g.*, Cebriá, 1992; López-Ruiz *et al.*, 1993). This fact is in agreement with structural studies showing that since the Variscan, the Iberian crust in the CVP has remained unstretched with regard to the neighboring areas of Central Spain (Vegas and Rincón-Calero, 1996). In addition, geological and geophysical data (Sánchez Vizcaino, 2008) preclude the existence of a Late Miocene sedimentary basin that would infill the "void" space yielded by the lithospheric stretching in the upper crust. Only epidermal, fluvial and lacustrine sediments, on average between 50 and 150 m in thickness increasing eastwards to the LMB (locally 550 m), cover the eroded cores of the km-scale Variscan folds which rule the Appalachian-type relief in central Spain.

Although the baby-plume hypothesis cannot be refuted, we suggest a more feasible alternative hypothesis for the origin of the volcanism of the rather small-sized, intraplate CVP compatible with the gravity models presented here. This hypothesis is mainly based on the coincidence in time of the CVP and the subduction-related Miocene volcanism in the south-eastern part of the Iberian Peninsula (Fig. 1). The subduction started in the Late Miocene in the SE of the Iberian Peninsula (Duggen *et al.,* 2004, 2005), and then migrated westward (Faccenna *et al.,* 2004 and references therein). This time linkage implies necessarily that the volcanism of the CVP occurred inside a NW-directed, generalized compressive regime which resulted in the stress transmission from the foreland fold-and-thrust belt of the External Betics, the external zone of the Betic Orogen in southern Spain (Fig. 13). In this context, the subduction-related volcanism of the south-eastern part of the Iberian Peninsula (2 in Fig.1 and SESVP in Fig. 13) is physically, but not geochemically linked to the specific intraplate volcanism of the CVP located in the Iberian foreland (CVP in Fig. 13). This linkage could be ascribed to the conceptual model recently proposed by Shin *et al.* (2012) for the generation of basaltic magma at the back-arc regions without extension. In our case study, this hypothesis has the following elements (Fig. 13):

-The Late Miocene tectonic setting when the volcanism occurred in the CVP consists of a NW-directed subduction of the intermediate Alboran Terrane under the south Iberian margin, yielding the magmatism in the SE of the Iberian Peninsula (Duggen *et al.,* 2004, 2005; SESVP in Fig. 13).

-This subduction also yielded a NW-directed transmission of compressive stresses in the upper plate and the formation of the External Betics (fold-and-thrust belt).

-The NW-transmitted compressive deformation yielded a gentle folding of the Iberian lithosphere with the formation of a swell in the Calatrava region which interferes with two roughly E−W-directed crustal folds, the Toledo Mountains and Sierra Morena ranges created in the Eocene-Oligocene (De Vicente and Vegas, 2009). In addition, as a secondary force, the vertical load of the thickened crust generated by the fold-and-thrust belt developed in the External Betics may also have contributed to generate folding in the thrusted lithosphere (Iberian Massif).

-The formation of the lithospheric folding in the Calatrava region results in a decrease of the pressure beneath the swell of the antiform that is likely to bring on basaltic magmatism along and below the swell. Shin *et al.* (2012) suggested that 1 km of amplitude in the folding in the LAB could yield

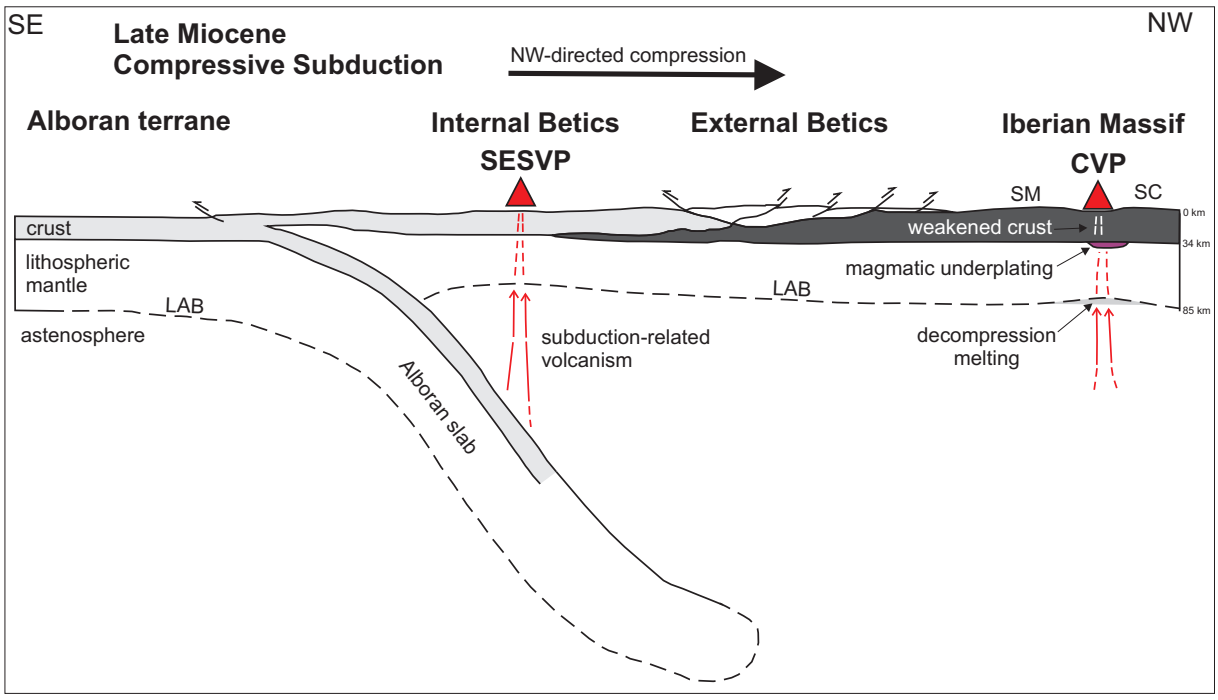

Fig. 13.- Conceptual model showing the spatial relations for the intraplate volcanism in the CVP in the Late Miocene compressional setting. Note that the internal zones of the Betics are formed by the upper crust of the Alboran terrane that becomes a part of the upper plate together with the Iberian Massif. Therefore the volcanism occurred in the CVP and in the SESVP is located in the upper plate during subduction. CVP= Calatrava Volcanic Province. SESVP= SE Spain Volcanic Province. SM= Sierra Madrona. SC= Sierra de la Calderina.

enough decompression to generate magmatism, but they remark that the uplifting rate during the lithospheric folding is more relevant. When the lithospheric folds are very gentle, the uplift rate is very fast, even for the case of very small horizontal convergence rates as between Africa and Iberia, and the decompression is more effective.

-In addition to the local decompression, if there is a pre-existing high upper mantle temperature in the CVP region, the generation of magmatism would be indeed more effective. Currie and Hyndman (2006) documented evidence that high upper mantle temperatures are not restricted to the collisional/subduction boundary but usually extend for several hundred kilometers in the retroarc foreland region, even in areas that have not undergone extension.

In addition to the aforementioned tectonic features, we consider that the occurrence of the localized volcanism in the CVP, with the volcanoes mostly aligned NW−SE, is also determined by the existence of the Variscan right-lateral shear band (Fig. 3), which yields a weakened crust that facilitates the ascent of the magmatic materials.

We therefore suggest that these features (Variscan right-lateral shear and gentle uparching of the Iberian lithosphere) explain better the magmatism in the CVP than previous hypotheses which are based on the stretching of the lithosphere. The combination of these features could be enough to produce localized magmatism which for the most part was stocked at the base of the crust in the form of an underplated body, as is supported by the gravity modeling (*i.e.*, sub-crustal anomalous density block); thereafter only a minor part of it reached the surface, but extending over a wide region. The activity of this mechanism ended when an oblique slab break occurred and simultaneously the subduction migrated westwards (*e.g.*, Faccenna *et al.*, 2004 and references therein), in the western Betics where a clear strain partitioning can be observed (*e.g.*, Pérez-Varela *et al.*, 2014 and references therein).

6. Conclusions

Gravity models do not support the rifting model adopted for the intraplate volcanism that occurred in the CVP because the crust shows an almost constant thickness with a very small northward thickening. This fact is in agreement with structural and geophysical studies showing that since the Variscan the Iberian crust in the CVP has remained unstretched with regard to the neighboring areas of Central Spain.

Gravity modeling suggests the existence of a sub-crustal anomalous low-density block beneath the CVP. This block could be underplated magmatic material stocked at the base of the crust suggesting that only a minor part of it intruded up into the upper crust and erupted, though it extended over a wide region.

With regard to the plume-related, non lithospheric origin invoked for the volcanism (*i.e.*, baby-plume hypothesis), it must be stressed that our gravity modeling is insensitive to changes in the depth of the LAB below ≈10 km at the vertical of the CVP. If a baby-plume exists beneath the CVP, it would be linked to a small lithosphere thinning undetectable from gravity modeling.

The localized magmatism of Calatrava can be related to the combination of two main factors:

One active, the gentle folding of the Iberian lithosphere and associated uplifting of the Variscan basement due to the NW-directed transmission of compressive stresses in the upper plate yielded by the subduction/collision in the south Iberian margin. The formation of the lithospheric folding in the Calatrava region results in a decrease of the pressure beneath the swell of the antiform that is likely to bring on basaltic magmatism along and below the swell.

One passive, the existence of a Variscan right-lateral shear band which yields a weakened crust that facilitates the ascent of the magmatic materials. The relatively small volume, but large extension, of the volcanic outcrops could be associated with the preferential ascent of the magmas along the weakened crust of the NW−SE-trending Variscan shear band.

Acknowledgements

We thank the Instituto Geográfico Nacional (IGN; National Geographical Institute), the Instituto Geológico y Minero de España (IGME; Geological Survey of Spain), the Empresa Nacional de Resíduos Radioactivos S. A. (ENRESA) and the Universidad Complutense de Madrid (UCM) for providing the gravity and topographic data. M. A. Sentre Domingo was funded by a grant of the IGN (Orden FOM/2824/2009). We express many thanks to A. Olaiz for his helpful comments on the earlier versions of the manuscript and the valuable revision and suggestions provided by P. Alfaro and an anonymous reviewer.

References

Álvarez García, J. (2002). Análisis gravimétrico e isostático en el Macizo Hespérico. *Diploma de Estudios Avanzados. Universidad Complutense de Madrid*, 73 p.

Ancochea, E. Giuliani, A., Villa, I. (1979). Edades radiométricas K-Ar del vulcanismo de la Región Central Española. *Estudios Geológicos* 35, 131–135.

Ancochea, E. Brändle, J.L. (1982). Alineaciones de volcanes en la región volcánica central española. *Revista de Geofísica* 38, 133–138.

Ancochea, E. (1999). El campo volcánico de Calatrava. *Enseñanza de las Ciencias de la Tierra* 7(3), 237–243.

Ancochea, E., Barrera, J.L., Bellido, F., Benito, R., Brändle, J.L., Cebriá, J.M., Coello, J., Cubas, C.R., De La Nuez, J., Doblas, M., Gómez, J.A., Hernán, F., Herrera, R., Huertas, M.J., López-Ruiz, J., Martí, J., Muñoz, M., Sagredo, J. (2004). Chapter VIII: Canarias y el vulcanismo neógeno peninsular. In: J.A. Vera, (ed.), *Geología de España*. Instituto Geológico y Minero de España, pp. 634–680. ISBN 84-7840-546-1.

Ayala, C. (2013). A new compilation of gravity data over the Iberian Peninsula and surrounding areas. *Internal Report TopoIberia Project (Consolider-Ingenio)*, 20 p. Instituto Geológico y Minero de España.

Azor, A., González Lodeiro, F., Simancas J.F. (1994). Tectonic evolution of the boundary between the Central Iberian and Ossa-Morena zones (Variscan Belt, SW Spain). *Tectonics,* 13, 45–61, doi:10.1029/93TC02724.

Barton, P.J., (1986). The relationship between seismic velocity and density in the continental crust—a useful constraint? *Geophys. J. R. Astron. Soc*. 87 (1), 195–208. doi: 10.1111/j.1365-246X.1986.tb04553.x

Bergamín, J.F., Carbó, A. (1986). Discusión de modelos para la Corteza y Manto superior en la zona sur del Área Centroibérica, basados en anomalías gravimétricas. *Estudios Geológicos* 42, 143–146.

Blakely, R.J. (1995). *Potential Theory in Gravity and Magnetic Applications*. Cambrid. Univ. Press. 448 p. ISBN 0-521-57547-8

Brocher, T.M. (2005). Empirical relations between elastic wavespeeds and density in the Earth's Crust. *Bulletin of the Seismological Society of America* 95(6), 2081–2092. doi: 10.1785/0120050077

Burg, J.-P., Iglesias, M., Laurent, P., Matte, P., Ribeiro A. (1981). Variscan intracontinental deformation: The Coimbra-Córdoba shear zone (SW Iberian Peninsula). *Tectonophysics,* 78, 161–177, doi:10.1016/0040-1951(81)90012-3.

Cebriá J.M. (1992). Geoquímica de las rocas basálticas y leucititas de la región volcánica de Campo de Calatrava, España. *Tesis Doctorales de la Universidad Complutense de Madrid,* 322 p.

Cebriá, J.M., Martín-Escorza, C., López-Ruiz, J., Morán-Zenteno, D.J., Martiny, B.M. (2011). Numerical recognition of alignments in monogenetic volcanic areas: examples from the Michoacán-Guanajuato Volcanic Field in Mexico and Calatrava in Spain. *J. Volcanol. Geotherm. Res*. 201, 73–82. doi:10.1016/j.jvolgeores.2010.07.016

Christensen, N.I. Mooney, W.D. (1995). Seismic velocity structure and composition of the continental crust: a global view. *Journal of Geophysical Research* 100(B7), 9761–9788.

Cloetingh, S., Burov, E., Beekman, F., Andeweg, B., Andriessen, P.A.M., Garcia Castellanos, D., de Vicente, G., Vegas, R. (2002). Lithospheric folding in Iberia. *Tectonics*, 21(5), 1–26.

Currie, C.A., Hyndman, R.D. (2006). The thermal structure of subduction zone back arcs. *J. Geophys. Res.* 111, B08404, doi:10.1029/2005JB004024.

Davis, M., Kusznir, N.J. (2004). Depth-dependent lithospheric stretching at rifted continental margins. In: G.D Karner (ed.), *Proceedings of NSF Rifted Margins Theoretical Institute*, pp. 92–136. Columbia University Press, New York.

De Vicente, G. Cloetingh, S. Muñoz-Martín, A. Olaiz, A. Stich, D. Vegas, R. Galindo-Zaldívar, J., Fernández-Lozano, J. (2008). Inversion of moment tensor focal mechanisms from active stresses around Microcontinent Iberia: Tectonic implications. *Tectonics* 27: 1-22. doi: 10.1029/2006TC002093

De Vicente, G., Vegas, R. (2009). Large-scale distributed deformation controlled topography along the western Africa-Eurasia limit: Tectonic constrains. *Tectonophysics* 474, 124–143. doi10.1016/j.tecto.2008.11.026.

Díez Balda, M.A., Vegas, R. (1992). La estructura de los pliegues verticales de la Zona Centro Ibérica. In: J.C. Gutiérrez-Marco, J. Saavedra, I. Rábano (eds.), *Paleozoico Inferior de Ibero-América*. Universidad de Extremadura, pp. 523–534.

Duggen, S., Hoernle, K., van den Bogaard, P., Harris C. (2004). Magmatic evolution of the Alboran region: The role of subduction in forming the western Mediterranean and causing the Messinian Salinity Crisis. *Earth Planet. Sci. Lett.* 218(1–2), 91–108. doi:10.1016/S0012-821X(03)006 32-0.

Duggen, S., Hoernle, K., van den Bogaard, P., Garbe-Schonberg, D. (2005). Post-collisional transition from subduction- to intraplate-type magmatism in the westernmost Mediterranean: Evidence for continental-edge delamination of subcontinental lithosphere. *J. Petrol.* 46(6), 1155–1201. doi:10.1093/petrology/egi013.

Ehsan, S.A., Carbonell, R., Ayarza, P., Martí, D., Martínez Poyatos, D.J., Simancas, J.F., Azor, A., Ayala, C.,Torné, M.,Pérez-Estaún, A. (2015). Lithospheric velocity model across the Southern Central Iberian Zone (Variscan Iberian Massif): The ALCUDIA wide-angle seismic reflection transect. *Tectonics* 34, 535–554, doi:10.1002/2014TC003661.

Ehsan, S.A., Carbonell, R., Ayarza, P., Martí, D., Pérez-Estaún, A., Martínez-Poyatos, D.J., Simancas, J.F., Azor, A., Mansilla, L. (2014). Crustal deformation styles along the reprocessed deep seismic reflection transect of the Central Iberian Zone (Iberian Peninsula). *Tectono-*

physics 621, 159–174, doi:10.1016/j.tecto.2014.02.014.

Faccenna, C., Piromallo, C., Crespo-Blanc, A., Jolivet, L., Rossetti, F. (2004). Lateral slab deformation and the origin of the western Mediterranean arcs. *Tectonics* 23, TC1012. doi:10.1029/2002TC001488

Fernández-Lozano, J., Sokoutis, D., Willingshofer, E., Dombrádi, E., Muñoz-Martín, A., De Vicente, G., Cloetingh, S. (2012). Integrated gravity and topography analysis in analog models: Intraplate deformation in Iberia. *Tectonics* 31, TC6005. doi:10.1029/2012TC003122.

Foulger, G.R. (2010). *Plates vs. Plumes: A geological controversy*. Wiley-Blackwell, 364 p. ISBN 978-1-4051-6148-0

García-Lobón, J.L., Rey-Moral, C., Ayala, C., Martín-Parra, L.M., Matas, J., Reguera M.I. (2014). Regional structure of the southern segment of Central Iberian Zone (Spanish Variscan Belt) interpreted from potential field images and 2.5 D modelling of Alcudia gravity transect. *Tectonophysics* 614, 185–202. dx.doi.org/10.1016/j.tecto.2013.12.005

Humphreys, E.R., Bailey, K., Hawkesworth, C.J., Wall, F., Najorka, J., Rankin, A.H. (2010). Aragonite in olivine from Calatrava, Spain—Evidence for mantle carbonatite melts from >100 km depth. *Geology* 38(10), 911–914. doi: 10.1130/G31199.1

Jacobsen, B.H. (1987). A case for upward continuation as a standard separation filter for potentialfield maps. *Geophysics* 52(8), 1138–1148. doi: 10.1190/1.1442378

López-Ruiz, J., Cebriá, J.M., Doblas, M., Oyarzun, R., Hoyos, M., Martín, C. (1993). Cenozoic intra-plate volcanism related to extensional tectonics at Calatrava, central Iberia. *Journal of the Geological Society of London* 150, 915–922.

Lustrino, M., Carminati, E. (2007). Phantom plumes in Europe and the circum-Mediterranean region. In: G.R. Foulger, D.M. Jurdy (eds.), Plates, plumes, and planetary processes. *Geol. Soc. Am. Special Paper* 430, 723–745. doi: 10.1130/2007.2430(33).

Lustrino, M., Wilson, M. (2007). The Circum-Mediterranean Anorogenic Cenozoic Igneous Province. *Earth Science Reviews* 81, 1–65. doi:10.1016/j.earscirev.2006.09.002

Martínez Poyatos, D., Carbonell, R., Palomeras, I., Simancas, J.F., Ayarza, P., Martí, D., Azor, A., Jabaloy, A., González Cuadra, P., Tejero, R., Martín Parra, L.M., Matas, J., González Lodeiro, F., Pérez-Estaún, A., García-Lobón, J.L., Mansilla, L. (2012). Imaging the crustal structure of the Central Iberian Zone (Variscan Belt): The ALCUDIA deep seismic reflection transect. *Tectonics* 31, 1–21.

Martos, Y.M., Galindo-Zaldívar, J., Catalán, M., Bohoyo, F., Maldonado, A. (2014). Asthenospheric Pacific-Atlantic flow barriers and the West Scotia Ridge extinction. *Geophysical Research Letters* 41, 1–7. doi:10.1002/2013GL058885

Mezcua, J., Gil. A., Benarroch, R. (1996). *Estudio gravimétrico de la Península Ibérica y Baleares*. Instituto Geográfico Nacional, Madrid. 11 p.

Muñoz-Martín, A., De Vicente, G., Fernández-Lozano, J., Cloetingh, S., Willingshofer, E., Sokoutis, D., Beekmanl, F. (2010). Spectral analysis of the gravity and elevation along the western Africa–Eurasia plate tectonic limit: Continental versus oceanic lithospheric folding signals. *Tectonophysics*, 495, 298–314. doi:10.1016/j.tecto.2010.09.036

Muñoz-Martín, A., De Vicente, G., Olaiz, A. J., Antón, L., Vegas, R., Granja Bruña, J.L. (2012). New on-line active stress map for the Iberian Peninsula from Seismic Moment Tensor earthquake focal mechanisms. *VIII Congreso Geológico de España*. *Geotemas* 13. p. 4.

Palomeras, I., Carbonell, R., Flecha, I., Simancas, J.F., Ayarza, P., Matas, J., Martínez Poyatos, D., Azor, A., González Lodeiro, F., Pérez-Estaún, A. (2009). Nature of the lithosphere across the Variscan orogen of SW Iberia: Dense wide-angle seismic reflection data. *Journal of Geophysical Research* 114, 1–29.

Palomeras, I., Carbonell, R., Ayarza, P., Fernàndez, M., Simancas, J.F., Martínez Poyatos, D., González Lodeiro, F., Pérez-Estaún, A. (2011). Geophysical model of the lithosphere across the Variscan Belt of SW-Iberia: multidisciplinary assessment. *Tectonophysics* 508, 42–51.

Palomeras, I., Thurner, S., Levander, A., Liu, K., Villasenor, A., Carbonell, R., Harnafi, M. (2014). Finite-frequency Rayleigh wave tomography of the western Mediterranean: Mapping its lithospheric structure. *Geochem. Geophys. Geosyst*. 15. doi:10.1002/2013GC004861.

Pérez-Valera, L.A., Sánchez-Gómez, M. Azor, A., Pérez-Valera, F. (2014). Quaternary activity of the structures associated with the Socovos fault system (Eastern Betics). In: J.A. Álvarez-Gómez, F. Martín González (eds.). Una aproximación multidisciplinar al estudio de las fallas activas, los terremotos y el riesgo sísmico. Segunda reunión ibérica sobre fallas activas y paleosismología, Lorca, (Murcia, España). pp. 35–38.

Rosenbaum, G., Lister, G.S., Duboz, C. (2002). Reconstruction of the tectonic evolution of the western Mediterranean since the Oligocene. In: G. Rosenbaum, G.S. Lister, (eds.), Reconstruction of the evolution of the Alpine-Himalayan orogeny. *Journal of the Virtual Explorer* 8, pp. 107–130.

Sánchez Vizcaíno, J. (2008). *Metodología para el estudio de cuencas intra-continentales de pequeño espesor. Aplicación de la misma en el anticlinorio de Ciudad real y en el sinclinorio de corral de Calatrava, Ciudad Real.* Tesis Doctoral, Universidad de Castilla-La Mancha. 599 p.

Sentre Domingo, M.A., Granja Bruña, J.L., Vegas Martínez, R., Sáinz-Maza, S. (2014). Análisis de anomalías gravimétricas y modelación cortical 2D de la región volcánica del Campo de Calatrava (Ciudad Real, España). *Geogaceta* 56, 43–46.

Shin, Y.H., Choi, K.S., Koh, J.S., Yun, S.H., Nakamura, E., Na, S.H. (2012). Lithospheric-folding-based understanding on the origin of the back-arc basaltic magmatism beneath Jeju volcanic island. *Tectonics* 31, TC4005. doi:10.1029/2011TC003092.

Simancas, J.F., Ayarza, P., Azor, A., Carbonell, R., Martínez Poyatos, D., Pérez-Estaún, A., González Lodeiro, F. (2013). A seismic geotraverse across the Iberian Variscides: orogenic shortening, collisional magmatism and orocline development. *Tectonics* 32(3), 417–432. dx.doi.org/10.1002/tect.20035.

Spector, A., Grant, F.S. (1970). Statistical models for interpreting aeromagnetic data. *Geophysics* 35, 293–302.

Stoppa, F., Rosatelli, G., Schiazza M., Tranquilli, A. (2012). Hydrovolcanic vs. Magmatic Processes in Forming Maars and Associated Pyroclasts: The Calatrava -Spain- Case History. In: Stoppa, F. (ed.) *Updates in Volcanology – A Comprehensive Approach to Volcanological Problems,* pp. 3–26. ISBN 978-953-307-434-4.

Talwani, M., Worzel, J.L., Landisman, M., (1959). Rapid gravity computations for two dimensional bodies with application to the Mendocino submarine fracture zone. *J. Geophys. Res.* 64, 49–59.

Talwani, M., Heirtzler, J.R., (1964). Computation of magnetic anomalies caused by two dimensional bodies of arbitrary shape. In: G.A. Parks, (ed.), Computers in the mineral industries, Part 1: *Stanford University Publications. Geological Sciences* 9, pp. 464–480.

Vegas, R., Roiz, J.M. (1979). La continuación hacia el Este de las estructuras hercínicas de las regiones de Las Villuercas, Guadalupe y Almadén (Zona Luso-Oriental Alcudiana). *Tecniterrae* 28, 1-5.

Vegas, R., Rincón-Calero, P.J. (1996). Campos de esfuerzos, deformación alpina y volcanismo Neógeno-cuaternario asociado en el antepaís bético de la provincia de Ciudad Real (España Central). *Geogaceta* 19, 31–34.

Won, I.J., Bevis, M. (1987). Computing the gravitational and magnetic anomalies due to a polygon: algorithms and Fortran subroutines. *Geophysics* 52, 232–238.

ONLINE SUPPLEMETARY MATERIAL

www. http://revistas.ucm.es/index.php/JIGE

Appendix A.- Model 4

Apendix B - Model 5